Mercury mobility, colloid formation and methylation in a polluted fluvisol as affected by manure application and flooding-draining cycle.

Lorenz Gfeller[1], Andrea Weber[1], Isabelle Worms[2], Vera I. Slaveykova[2], Adrien Mestrot[1]

[1]Institute of Geography, University of Bern, Hallerstrasse 12, 3012 Bern, Switzerland
[2]Environmental Biogeochemistry and Ecotoxicology, Department F.-A. Forel for environmental and aquatic sciences, School of Earth and Environmental Sciences, Faculty of Sciences, University of Geneva, Uni Carl Vogt, Bvd Carl-Vogt 66, CH-1211 Geneva 4, Switzerland
Correspondence to: Adrien Mestrot (adrien.mestrot@giub.unibe.ch)

Abstract

Floodplain soils polluted with high levels of mercury (Hg) are potential point sources to downstream ~~eco-systems~~ecosystems. Repeated flooding (e.g. redox cycling) and agricultural activities (e.g. organic matter addition) may influence the fate and speciation of Hg in these soil systems. The formation and aggregation of colloids and particles influences both Hg mobility and its bioavailability to methylmercury (MeHg) forming microbes. In this study, we conducted a microcosm flooding-draining experiment on Hg polluted floodplain soils originating from an agriculturally used area situated in the Rhone Valley (Valais, Switzerland). The experiment comprised two 14 days flooding periods separated by one 14 days draining period. The effect of freshly added natural organic matter on Hg dynamics was assessed by adding liquid cow manure (+MNR) to two ~~control~~ soils characterized by different Hg (47.3 ± 0.~~56~~ mg kg^{-1} or 2.38 ± 0.01 mg kg^{-1}) and organic carbon (OC: 1.92 wt. % or 3.45 wt. %) contents. During the experiment, the release, colloid formation of Hg in soil solution and ~~methylation~~ the net MeHg production ~~of Hg~~ in the soil ~~solution~~ were monitored. Upon manure addition in the highly polluted soil (~~lowest~~lower OC), an accelerated release of Hg to the soil solution could be linked to a fast reductive dissolution of Mn oxides. The manure treatments showed a fast sequestration of Hg and a higher percentage of particulate (0.02 – 10 µm) bound Hg. As well, analyses of soil solutions by asymmetrical flow field-flow fractionation coupled with inductively coupled plasma mass spectrometry (AF4–ICP–MS) revealed a ~~proportional~~ relative increase of colloidal ~~-DOM-~~Hg bound to dissolved organic matter (Hg-DOM) and inorganic colloidal Hg (~~+MNR:~~ 70 - 100 %) ~~; control: 32 – 70 %)~~ upon manure addition. Our experiment shows ~~that net Hg methylation~~a net MeHg production ~~(MeHg/Hg) was highest after~~ the first flooding and draining period and a subsequent decrease~~d again~~ in absolute MeHg concentrations after the second flooding period. Manure addition did not ~~No significant effects~~ change ~~on~~ net MeHg production significantly ~~methylation upon manure addition was found~~in the incubated soils. The results of this study suggest that manure addition may promote Hg sequestration by Hg complexation on large organic matter components and the formation and ~~/~~aggregation of inorganic $HgS_{(s)}$ colloids in Hg polluted fluvisols with low levels of natural organic matter.

Formatted: Not Highlight

Formatted: Not Highlight

Formatted: Not Highlight

Formatted

Copyright statement (will be included by Copernicus)

1. Introduction

Mercury (Hg) is a pollutant of global concern due to its high toxicity and to its global biogeochemical cycle which spans all environmental compartments (atmosphere, oceans, soils etc.) (Beckers and Rinklebe, 2017; AMAP/UN Environment, 2019). Sediments and soils are major Hg pools with relatively long residence times (Amos et al., 2013; Driscoll et al., 2013). Legacy Hg from industrial sites (e.g. chloralkali plants or mining areas) retained in soils are a key source for present day atmospheric Hg (Amos et al., 2013). However, this retained Hg pool can also be remobilized by landscape alteration, land use (e.g. fertilization, manure addition) or climate induced changes such as drought-flood-drought cycles of soils (Singer et al., 2016). These inputs are a threat to downstream ecosystems and human health due to release of inorganic Hg and the formation and bioaccumulation of toxic monomethylmercury (MeHg) in both aquatic and terrestrial food chains (Bigham et al., 2017).

Mercury is redox sensitive and occurs mainly as elemental Hg^0, inorganic Hg^{2+} or in the form of MeHg in soils. In general, Hg speciation in soils depends on the biogeochemical conditions. For example, in natural organic matter (NOM) rich boreal peatlands and forest soils, Hg is primarily bound to thiol-groups of NOM (NOM–Hg), associated with $FeS_{(s)}$ or found as cinnabar ($HgS_{(s)}$) or meta-cinnabar (ß-$HgS_{(s)}$).~~or found as $FeS_{(s)}$ or as cinnabar $HgS_{(s)}$.~~ These species are the thermodynamically most favored forms of Hg in these environments (Skyllberg et al., 2006; Skyllberg and Drott, 2010; Biester et al., 2002). However, Hg sorbed on the surfaces of manganese (Mn), iron (Fe) and aluminum (Al) oxy-hydroxides may also represent important Hg-pools in soils with low amounts of NOM (Guedron et al., 2009).

The fate of Hg in soils is still not well characterized, and its mobilization and sequestration in soil depends on a variety of factors and mechanisms. The release of Hg to the soil solution and its further transport has been associated with the mobilization of NOM (Kronberg et al., 2016; Eklöf et al., 2018; Åkerblom et al., 2008), copper (Cu) nano-particles (Hofacker et al., 2013) or the reductive dissolution of Fe/Mn-oxyhydroxides (Frohne et al., 2012; Gygax et al., 2019; Poulin et al., 2016). Earlier studies reported a~~n~~ relatively rapid ~~immediate~~ decrease of dissolved Hg after its release upon flooding in various riparian settings (Hofacker et al., 2013; Poulin et al., 2016; Gygax et al., 2019). Possible pathways for this decrease are Hg^{2+} reduction to Hg^0, sorption to recalcitrant NOM, formation of meta-cinnabar ß-$HgS_{(s)}$ or co-precipitation of Hg in ~~sulfi~~sulphides (e.g. $FeS_{(s)}$) or metallic particles.

Metallic colloids in soil may be formed by ~~e.g.~~ biomineralization during soil reduction or precipitation in the root zone and potentially incorporate toxic trace elements like Hg (Weber et al., 2009; Manceau et al., 2008). These colloids may increase the mobility and persistence of toxic trace metals in soil solution if they do not aggregate to bigger particles. During a flooding incubation experiment, Hofacker et al. (2013) observed the incorporation of Hg in Cu nano-particles, which were shown to be formed by ~~formed by biomineralization~~ fermetive bacteria species (Hofacker et al., 2015). Colloidal ß-$HgS_{(s)}$ has been reported to form abiotically in soils under oxic conditions directly by interaction with thiol-groups of NOM (Manceau et al., 2015). In solution, Dissolved Organic Matter (DOM) has a major influence in the formation and aggregation of metallic colloids and particles. It may promote the dissolution of $HgS_{(s)}$ phases ~~,~~ (Miller et al., 2007; Ravichandran et al., 1998) ~~or decelerate~~decelerate the aggregation and

Formatted: Font color: Auto, English (United Kingdom), Not Highlight

Formatted: Font color: Auto, Not Highlight

growth of $HgS_{(s)}$~~Hg incorporating metal sulfide~~ colloids as well as affect the crystallinity of $HgS_{(s)}$ phases ~~by complexing Hg ions as well as altering the reaction kinetics of e.g. $HgS_{(s)}$ formation~~(Miller et al., 2007; Ravichandran et al., 1998; Gerbig et al., 2011; Poulin et al., 2017; Pham et al., 2014). ~~The~~ Same effects ~~were~~as also observed for other metal ~~sulfi~~sulphide-, oxide- or carbonate colloids (Aiken et al., 2011; Deonarine et al., 2011). In case of Hg, inhibition of ß-$HgS_{(s)}$ ~~this~~ formation may in turn increase its mobility and bioavailability to MeHg producing microorganisms (Deonarine and Hsu-Kim, 2009; Ravichandran et al., 1999; Aiken et al., 2011; Graham et al., 2012). Chelation of Hg with higher molecular weight ~~larger~~ NOM ~~molecules~~ may as well inhibit the microbial availability of Hg (Bravo et al., 2017). Within Hg–NOM, ~~the sorption on larger~~ hydrophobic, thiol -rich NOM with higher molecular weight contain a higher density of strong sorption sites (thiol groups) ~~is thermodynamically favored~~(Haitzer et al., 2002). However, different ligand exchange reactions (e.g. carboxyl-groups to thiol groups) kinetically control this sorption and thus the bioavailability of dissolved Hg in aqueous systems (Miller et al., 2007; Miller et al., 2009; Liang et al., 2019). The partly contradicting statements above illustrate the complex role of NOM and DOM on the Hg cycle and Hg bioavailability and the need for more research in this field.

The formation of MeHg from inorganic Hg^{2+} has been shown to be primarily microbially driven. Environments of redox oscillation (e.g. floodplains, estuaries) represent hot spots for Hg methylation (Marvin-DiPasquale et al., 2014; Bigham et al., 2017). Mercury methylators are usually anaerobe microbial species such as ~~sulfate~~sulphate reducers (SRB), Fe reducers (FeRB), archaea and some firmicutes (Gilmour et al., 2013). Generally, Hg is bioavailable to methylators in the form of dissolved Hg^{2+}, Hg complexed by labile DOM, Hg bearing inorganic nanoparticles (e.g. $FeS_{(s)}$, $HgS_{(s)}$) but is less available when complexed by particulate organic matter (Hg–POM) or larger inorganic particles (Chiasson-Gould et al., 2014; Graham et al., 2013; Rivera et al., 2019; Zhang et al., 2012; Jonsson et al., 2012). Further, DOM is a main driver of Hg methylation as it influences both bioavailability and microbial activity. The role of DOM as electron donor may enhance the microbial activity and thus the cellular uptake. The composition and origin of DOM were reported to change Hg methylation rates (Drott et al., 2007; Bravo et al., 2017). For example, ~~(~~Bravo et al.~~,~~ (2017) showed that in lake sediments, terrestrial derived DOM led to slower methylation rates than phytoplankton derived DOM. The addition of DOM in form of organic amendments (e.g. manure~~, or~~ rice straw, biochar) ~~had~~ has been reported to have both an enhancing (Gygax et al., 2019; Liu et al., 2016; Wang et al., 2019; Eckley et al., 2021; Wang et al., 2020) or no effect (Zhu et al., 2016; Liu et al., 2016) on the ~~net methylation~~net MeHg production in soils. Further, organic amendments were reported to shift microbial communities. Both the enhancement of Hg demethylators, Hg reducers (Hu et al., 2019) as well as the enhancement Hg methylators upon organic amendments were reported (Tang et al., 2019; Wang et al., 2020). Environments of ~~M~~elevated Hg methylation (riparian zone, estuary) are ~~hotspots (redox boundaries) are~~ also ~~places~~ places of elevated NOM degradation and mineralization due to temporal changes in redox conditions. The degradation of large NOM to more bioavailable low molecular weight (LMW) compounds promoted by microbial Mn oxidation, especially in systems with neutral pH (Jones et al., 2018; Sunda and Kieber, 1994; Ma et al., 2020), is also hypothesized to increase bioavailability of Hg–NOM. However, amendments of Mn oxides were also shown to inhibit Fe, SO_4^{2-} reducing conditions and thus MeHg formation in sediments (Vlassopoulos et al., 2018).

Field Code Changed

Formatted: German (Switzerland)

Field Code Changed

Formatted: Superscript

Hg methylation and mobilization is intensively studied in paddy field soils and peat soils due to their relevance in food production or the Hg global cycle (Wang et al., 2019; Tang et al., 2018; Liu et al., 2016; Hu et al., 2019; Wang et al., 2016; Zhao et al., 2018; Zhu et al., 2016; Kronberg et al., 2016; Skyllberg, 2008; Skyllberg et al., 2006). However, only few studies focused on Hg methylation and mobility in temperate floodplain soils (Frohne et al., 2012; Hofacker et al., 2013; Gilli et al., 2018; Poulin et al., 2016; Lazareva et al., 2019; Wang et al., 2020; Beckers et al., 2019). As well, few studies have examined the effect of flooding and/or land use (NOM addition in the form of animal manure) in polluted soils with respect to Hg release and methylation potential (Tang et al., 2018; Gygax et al., 2019; Zhang et al., 2018; Hofacker et al., 2013; Frohne et al., 2012). Furthermore, most of these studies were focusing on soils with rather high OC levels (5 – 10 wt. %) and only few researchers have addressed the decrease of Hg in soil solution of flooded soils over time, including the fate of colloidal Hg.

This work focused on the effect of the agricultural practices on the Hg mobility ~~biogeochemistry~~ and methylation in a real-world contaminated fluvisol with specific emphasis on the flooding-draining cycle and manure addition. By conducting microcosm experiments, ~~We~~ we studied the effect of these cycles and manure addition on 1.) the release and sequestration of Hg, 2.) the ~~net~~ methylation of Hg and 3.) the evolution of colloidal and particulate Hg in soil solution. ~~,~~ The latter was studied by analyzing different soil solution filter fractions (0.02 and 10 µm~~0.02/10 µm~~) as well as analyzing selected samples by asymmetric flow field flow fractionation coupled to a UV_{vis} detector, a fluorescence detector and an ICP–MS (AF4–ICP–MS). Based on the presented state of knowledge, we hypothesise that the manure addition would accelerate the release of Hg by accelerated reductive dissolution of Mn- ~~-~~oxyhydroxides in these soils and eventually change Hg speciation in the system towards Hg-NOM complexes and ß-$HgS_{(s)}$ colloids.

Field Code Changed

Formatted

2. Methods and Materials

2.1. Sample collection

We sampled soil from agriculturally used fields in the alpine Rhone Valley in Wallis, Switzerland on September 30th, 2019. The fields are situated in a former floodplain next to the artificial "Grossgrundkanal" canal. This canal was built in the 1900s to drain the floodplain and as a buffer for the waste water releases ~~emissions~~ of an ~~acetaldehyde producing~~ chemical plant upstream historically using Hg in different processes (chlor-alkali electrolysis, acetaldehyde- and vinyl chloride production) ~~upstream~~. The soils on the floodplain were subjected to Hg pollution from this plant between the 1930s and the 1970s, mostly through the removal and dispersion of the canal sediments onto the agricultural fields (Glenz and Escher, 2011). After heavy rain events, the fields are subjected to draining-flooding cycles (Fig. ~~S1~~S1) and have been identified as potential hotspots for Hg methylation and release (Gygax et al., 2019). For this study, soil was sampled from a cornfield and a pasture field next to the canal. A map and the coordinates of the sampling locations is provided in the supplement (Fig. S1~~1~~, Table S1). At each site, a composite sample of approx. 10 kg of soil was sampled between 0 – 20 cm depth from ten points on the fields. The soil samples were named after their relative pollution and organic carbon levels (High Mercury, Low Carbon (HMLC) and Low Mercury, High Carbon (LMHC), see Part 4.3 below for details on the soils. After sampling, roots were removed, and the fresh soil was sieved to < 2 mm grain size, further homogenized, split in two parts and stored on ice

in airtight PE Bags for transport to the laboratory. Additionally, approx. 2 L of liquid cow manure was sampled from a close-by cattle farm. One aliquot of the samples was stored at - 20° C until further processing. The remaining part was used for the incubation experiment within 12 h after sampling. A detailed description of the site and sampling procedures is given in the supplement (Sect. S1).

2.2 Microcosm Experiments~~Incubation experimental setup.~~

An initial incubation was conducted in 10 L HDPE containers in the dark for seven days in an atmosphere of 22 °C and 60 % relative humidity (RH) in order to equilibrate the soils and to prevent a peak of microbial respiration induced by the soil sieving before the onset of the experiment (Fig. 1). After the initial incubation period soils were used in the flooding and draining experiments, which were conducted in 1 L borosilicate glass aspirator bottles (Fig. S2). ~~After this initial incubation the soils were passed to the flooding-draining experiment. This was conducted in 1 L Borosilicate aspirator bottles.~~ The environment created through ~~though~~ soil flooding in these bottles will be called microcosm (MC) in the following text. Microcosm experiments were performed in experimental triplicate ~~The experiments were run in triplicates~~ and named after the relative Hg- ~~pollution~~ and organic carbon levels of the used soil (HMLC and LMHC) and ~~and~~ the treatment with or without manure addition (added ~~control and~~ +MNR). The MCs were equipped with an acid washed suction cup with a pore size of < 10 µm (model: 4313.7/ETH, ecoTech Umwelt-Meßsysteme GmbH, Bonn, Germany). In the following sequence, 700 g of artificial rainwater (NH_4NO_3 11.6 mg L^{-1}/ K_2SO_4 7.85 mg L^{-1}/ Na_2SO_4 1.11 mg L^{-1}/ $MgSO_4 \cdot 7H_2O$ 1.31 mg L^{-1}/ $CaCl_2$ 4.32 mg L^{-1}) ~~were~~ was added to the MCs. For the manure treatment, 0.6 % (w/w) (3 g) of liquid cow manure was added to the MCs corresponding to one application of liquid manure on a cornfield following the principles of fertilization of agricultural crops in Switzerland (Richner and Sinaj, 2017) and finally fresh soil was added with a $soil_{dry}$:water ratio of 1:1.4 (w/w) (Fig. S~~3~~2). Then, the MCs were gently shaken for at least one minute to ~~avoid~~ remove any remaining air bubbles in the soil and pore space. An additional mixture of fresh soil artificial rainwater (1:1.4 (w/w)) was shaken for 6 h to assess the equilibration of the solid and liquid phase during the experiment. The MCs were covered with Parafilm®, transferred to the incubation chamber (APT.line™ KBWF, Binder, Tuttlingen, Germany) and incubated in the dark for 14 days in atmosphere of 22 °C and 60 % RH. The incubation temperature was chosen to be close to the daily mean soil temperature in 10 cm depth during summer months between 2015–2019 (21.4 °C) at the closest soil temperature monitoring station (Sion, VS, provided by MeteoSwiss) situated downstream. After the first flooding period, the supernatant water was pipetted off, and remaining water was sampled through the suction cups to drain the MCs. They were weighted before and after water removal. Then, approximately 25 g of moist soil was sampled by two to three scoops though the whole soils column using a disposable lab spoon. The MCs were kept drained in an atmosphere of 22 °C and 10 % RH for 14 days. For the second flooding period, the MCs ~~incubators~~ were again flooded with 500 g of artificial rainwater and incubated for another 14 days in an atmosphere of 22 °C and 60 % RH (Fig. 1). After the incubation, the suction cups were removed, the soils were homogenized and then transferred from the MC to a PE bag and stored at -20 °C until further processing.

2.3 Soil and manure characterization

Frozen soil and manure samples were freeze dried to avoid a loss of Hg prior to analyses (Hojdová et al., 2015), ground using an automatic ball mill (MM400, Retsch, Haan, Germany) and analyzed for the following chemical parameters. Carbon (C), nitrogen (N) and sulfur (S) were measured with an elemental analyzer (vario EL cube, Elementar Analysensysteme, Langenselbold, Germany). Organic Carbon (OC) was calculated by subtracting the C concentration of a loss on ignition sample (550 °C for 2 h) from the original C concentration~~.~~. pH was measured in an equilibrated 0.01 M $CaCl_2$ solution (1:5 soil:liquid ratio). Mineral composition was measured by X-ray diffraction (XRD, CubiX^3, Malvern Panalytical, Malvern, United Kingdom). Trace and major metals (e.g. Fe, Mn, Cu) and Hg were extracted from soils using a 15.8 M nitric acid microwave digestion and measured using an Inductively Coupled Plasma - Mass Spectrometer (ICP–MS, 7700x, Agilent Technologies, Santa Clara, United States of America). Methylmercury was selectively extracted with HCl and dichloromethane (DCM) using an adapted method described elsewhere (Gygax et al., 2019). We modified this method to achieve high throughput (64 Samples per run) and measurements by High Pressure Liquid Chromatography (HPLC, 1200 Series, Agilent Technologies, Santa Clara, United States of America) coupled to the ICP–MS. Details on laboratory materials, extractions, analytical methods and instrumentation are provided in the supplement (Sects. S2, S3). The change in MeHg concentration in the MCs were likely a result of the simultaneous production and degradation of MeHg. Thus, the term "net MeHg production" was used to represent these processes. We calculated the relative net MeHg production ~~de-/methylation~~ during the incubation as the relative difference of MeHg/Hg ratios between two time points (t) using Eq. (1).

$$net\ MeHg\ production\ (\%) = \frac{\left(\frac{MeHg}{Hg}_{t_{i-1}} - \frac{MeHg}{Hg}_{t_i}\right)}{\frac{MeHg}{Hg}_{t_{i-1}}} \times 100 \quad (1)$$

2.4 Soil description

Both soils were identified as *Fluvisols gleyic.* They have a silt loam texture, the same mineral composition but differing Hg and organic carbon (C_{org}) concentrations (Table 1). For elements relevant for Hg cycling, Hg molar ratios (Hg:Cu, Hg:C_{org}, Hg:Mn) differ between samples and soils used in similar incubation experiments (Hofacker et al., 2013; Poulin et al., 2016). We note that the $[C_{org}/Mn]_{molar}$ was 30 % higher in the LMHC soil compared to HMLC. X-Ray diffractograms of both soils are shown in Fig. S43. The soils diffractograms are overlapping each other and the qualitative analyses of the diffractograms show that the soils parental material is composed of the same five main mineral phases, q~~Q~~uartz, ~~Albite~~albite, ~~Orthoclase~~orthoclase, ~~Illite~~illite/~~Muskovite~~muskovite, ~~Calcite~~calcite.

2.5 Soil solution sampling and analyses

Soil solution was sampled 0.25, 1, 2, 3, 4, 5, 7, 9, 11, 14 days after the onset of each flooding period respectively (Fig. 1, Fig. S54). It was sampled though the tubing connected to the suction cup (< 10 µm pre size). The first 2 ml were sampled with a syringe and discarded to prime the system and condition the tubing. After, 4 ml were drawn through an airtight flow-through system to measure the redox potential (Hg/HgCl ORP electrode) and pH. Then,

approximately 35 ml of soil solution were sampled using a self-made syringe pump system allowing for a regular flow and minimal remobilization of fine particles. Like this, 4-6 % of the added artificial rainwater volume was sampled at each sampling point (Fig. S3). Throughout the experiment the soils remained entirely submerged. At each sampling time, sample splits were preserved without further filtration~~We left one part of the soil solution as such~~ (~~filtered by suction cup to~~ < 10 µm) and filtered at 0.02 µm ~~while a second part was filtered to < 0.02 µm pore size~~ (Whatman® Anodisc 0.02 µm, Sigma-Aldrich, St. Louis, United States of America). Additionally, at 2,5 and 9 days an additional sample split was filtered at ~~A third part was filtered to <~~ 0.45 µm (Polytetrafluoroethylene Hydrophilic, BGB, Boeckten, Switzerland) for colloid characterization.~~µm on days 2, 5 and 9 after the onset of each flooding period.~~ Incubation experiment blanks were taken by sampling MilliQ water through from an empty 1 L borosilicate aspirator bottle 3 times throughout the experiment. Subsequently, the samples were subdivided and treated for different analyses. They were preserved in 1 % HNO_3 for multi elemental analysis (~~Al, P, Cr,~~ Mn, Fe, ~~Ni,~~ Cu, ~~Zn,~~ As~~, Sr, U~~) and in 1 % HNO_3 and 0.5 % HCl for Hg analysis and analyzed by ICP–MS. For major anion (Cl^-, NO_3^-, SO_4^{2-}) and cation (K^+, Na^+, Mg^{2+}, Ca^{2+}) measurements, samples were diluted 1:4 in ultra-pure water and analyzed by Ion Chromatography (Dionex Aquion™, Thermo Fisher Scientific Inc., Waltham, United States of America). Samples for Dissolved Organic Carbon (DOC), Particulate Organic Carbon POC and Total Nitrogen Bound (TN_b) were diluted 1:5 and stabilized using 10 µl of 10 % HCl and measured using an Elemental Analyzer (vario TOC cube, Elementar Analysensysteme, Langenselbold, Germany). Incubation experiment blanks were below ~~0.396~~4.75 mg L^{-1} ~~mM~~ and 22.4~~1.6~~ ~~µM~~ µg L^{-1} for DOC and TN_b, respectively. These relatively high blank values might originate from either the syringes or the suction cups (Siemens and Kaupenjohann, 2003). Uncertainties of soil solution parameters are displayed as 1SD of the triplicate incubation experiments throughout the manuscript. HCO_3^- concentrations were estimated based on the ionic charge balance of the soil solution using VisMinteq (https://vminteq.lwr.kth.se/). A detailed schedule and list of analyses is provided in Figure 1~~ and Table S2~~. Concentrations of specific filtered ~~filter~~ fractions are labelled with ~~suffix~~ subscripts (e.g. $HgT_{<0.02µm}$) for all measured metals. Particulate concentrations (0.02 µm < X < 10 µm) (e.g. P-~~Hg~~Fe) and its proportion to the total (e.g. P-~~Hg~~~~rel~~Mn_{rel}) were determined as the difference between unfiltered and filtered concentration (Table 2~~1~~).

Formatted: Not Highlight

Formatted: Not Highlight

Formatted: Superscript, Not Highlight

Formatted: Not Highlight

Formatted: Superscript

Formatted

2.6 Characterization of Colloids (AF4)

An aliquot of the soil solution was used for characterization of colloids in one out of three replicate MCs (Rep1) of each treatment on days 2, 5, 9 days after the onset of each flooding period respectively. Right after sampling, the aliquots were transferred to a N_2 atmosphere in a glove box. There, the samples were filtered to < 0.45 µm and preserved in airtight borosilicate headspace vials at 4 °C. Colloidal size fractions and elemental concentrations of the filtrates were analyzed by Asymmetrical Flow Field-Flow Fractionation (AF4, AF2000, Postnova analytic, Landsberg am Lech, Germany) coupled to a UV_{254nm} absorbance detector (UV, SPD-M20A, Shimazu, Reinach, Switzerland~~UVD~~), a Fluorescence detector (FLD, RF-20A, Shimazu, Reinach, Switzerland) and an ICP–MS (7700x, Agilent Technologies, Santa Clara, United States of America) within 14 days after sampling. Colloids contained in 1 mL of samples were separated in a channel made of a trapezoidal spacer of 350 µm thickness and a regenerated cellulose membrane with a nominal cut-off of 1 kDa used as accumulation wall. The mobile phase used for AF4

Formatted: English (United States)

elution was 10 mM NH_4NO_3 at pH 7 and was degassed prior entering the channel by argon flowing. A linear decrease of crossflow from 2 to 0 mL min^{-1} over 20 min was used after injecting the samples at an initial crossflow of 2.7 mL min^{-1}. At the end of a run, the crossflow was kept at 0 mL min^{-1} for 5 min in order to elute non-fractionated particles. Retention times were transformed into hydrodynamic diameters (d_h) by an external calibration using Hemocyanin Type VIII from Limulus polyphemus hemolymph (monomer d_h = 7 nm, Sigma-Aldrich) and ultra-uniform gold nanoparticles (Nanocomposix) of known d_h (19 nm and 39 nm). Additionally, the elution of the smallest retention times (d_h < 10 nm) were converted into molecular masses (Mw) using PSS standards (Postnova analytic, Landsberg am Lech, Germany) with Mw ranging from 1.1 to 64 kDa (Fig. S6~~5~~), using AF4-UVD_{254nm}.

Fractograms obtained in Counts Per Seconds (CPS) from Time Resolved Analysis (TRA) acquisition were converted to µg L^{-1} using external calibrations made from a multi-element standard solution (ICP multi-element standard solution VI, Merk, Darmstadt, Germany) diluted in 1 % HNO_3 or a Hg standard (ICP inorganic Hg standard solution, TraceCERT®, Sigma-Aldrich, St. Louis, United States of America) diluted in 1.0 % HNO_3 and 0.5 % HCl~~0.5 % HCl 1 % HNO_3~~. The different size fractions were obtained by multiple extreme-shaped peak fitting, using OriginPro 2018 software (OriginLab Corporation). The peaks obtained were then integrated individually, after conversion of elution time to elution volume, to provide the quantity of Hg in each size fractions (Dublet et al., 2019). The analytes passing the 1 kDa membrane are considered as the (< 1 kDa) truly dissolved fraction. It was calculated by subtracting the concentrations of colloidal HgT recovered by AF4–ICP–MS (total integration of the Hg signals) to the total dissolved HgT concentrations measured separately by ICP–MS in corresponding acidified samples. The concentration of truly dissolved Hg is displayed as $HgT_{<1kDa}$ for the rest of the article (Table 1). AF4–ICP–MS, UV_{254nm} and fluorescence signals were used to further characterize Hg bearing colloids, after hydrodynamic size separation by AF4. The UV_{254nm} light absorption is widely used to detect organic compounds but it should be noted that part of the UV_{254nm} light signal can as well originate from Fe(II) or Fe hydroxides (Dublet et al., 2019). This was not the case in this study since UV_{254nm} signals ~~were~~ co-eluted ~~associated~~ with C signals recorded by ICP–MS and matched the fractograms obtained by the FLD detector tuned at the wavelengths specific for humic-like fluorophores. It is therefore assumed that UV_{254nm} signal represents organic compounds throughout the manuscript.

3. Results

3.1 ~~Pore water~~Soil solution chemistry and Hg dynamics

In the HMLC MCs, the pH of the soil solutions remained in a neutral to alkaline range of 8 to 8.4 during the ~~incuab-tion~~incubation experiment (Fig. S7). ~~The DOC concentration ranged between 37.5 and 106 mg L^{-1} (Fig.).~~ A continuous soil reduction was observed (Fig. 2a). Soil solution NO_3^- depletion was observed during the first 7 days of incubation (Fig. 2b). Nitrate was under detection limit for the second flooding phase ~~together with the onset of Mn release at day 7 of the main incubation~~. At day 7, Mn concentrations increased ~~at day 7~~ together with a marginal increase of Fe (Figs. 2c-f~~)~~ ~~started between day 7 and 9~~. This was coincided with a decrease of the relative particulate fraction ($P\text{-}Mn_{rel}$ and $P\text{-}Fe_{rel}$) of these metals. Release of Mn and Fe were assumed to mark the onset of reductive dissolution of Mn- and Fe--oxyhydroxides. The decrease in ssulphate (SO_4^{2-}) concentration could not be used to

Formatted: English (United States)

Formatted: Subscript

Formatted: Subscript

Formatted: Subscript

Formatted: Superscript

assess the onset of of sulphate reduction. This is due to a chemical gradient between supernatant water and soils solution demonstrated by the continuous decrease in concentration of conservative ions (Cl^-, Na^+, K^+) (~~Fig. S ;~~Sect. 4.4). To monitor sulphate reduction, we ~~monitored~~use the molar ratios of SO_4^{2-} to Cl^- (Fig. 2g). Sulphate to chloride ratios stood constant during the first flooding and slightly increased at the onset of second flooding phase. This suggests that no sulphate reduction took place in the HMLC MCs during ~~both flooding phases~~the whole experiment. The DOC concentration ranged between 37.5 and 106 mg L^{-1} (Fig. 2h). ~~The DOC concentration ranged between 37.5 and 106 mg L^{-1} (Fig.).~~Both $HgT_{<0.02\mu m}$ and $HgT_{<10\mu m}$ concentrations remained low between day 0-5 (Phase 0), then increased together with the Mn release between days 5-11 (Phase 1) and decreased between ~~during the draining days~~ 14-29 (Phase 2) during the draining period (Fig. 3a). The relative fraction of particulate HgT ($P\text{-}HgT_{rel.}$), gradually decreased from a maximum of 88 % to a minimum of 25 % during phase 0 and phase 1, but increased again to 60-77 % during phase 2 (Fig. 3b-c). $Cu_{<0.02\mu m}$ concentrations increased up to 88.2 ± 17.5µg L^{-1} within the first 4 days and then gradually decreased to 30.6 ± 3.54 µg L^{-1} at day 14 (Fig. 4a). Arsenic concentrations simultaneously increased with the release of Fe during the whole incubation (Fig. 4b).

During the second flooding period, individual MCs behaved differently in the HMLC ~~control treatment~~run. The differences of soil solution E_h and redox sensitive metals (e.g. Mn, Fe, Hg, Cu) were apparent from the start of the second flooding (Figs. ~~2 2c f~~-f, 3a-c, 4a~~g, S8~~). Contrastingly, DOC concentrations and pH remained similar between incubators (Figs. 2h, S7~~h~~). One replicate (Rep1) showed a pronounced increase of ~~E_h~~redox potential after the draining period (Fig. 2a~~i~~). The E_h remained high (150 to 300 mV) for the whole second flooding period. A depletion and subsequent release of Mn in soil solution was observed, indicating the formation and redissolution of Mn ~~oxide~~oxyhydroxide minerals (Fig. 2c-d). Subsequently, $Mn_{<0.02\mu m}$ increased and peaked at 448 µg L^{-1} ~~in Rep1 at the end of the experiment~~by the end of the experiment in Rep1. The E_h of Rep2 was lower (between 28 and 120 mV), Mn concentrations did not decrease during the draining phase, and a release of Fe was observed during the second flooding phase indicating the reduction of Fe oxyhydroxides. Rep3 had a E_h in the range of Rep2 but neither a rerelease of Mn nor a release of Fe was observed during the second flooding phase. Also, HgT behaved differently within incubators during the second flooding period. Between days 29-42 (Phase 3), $HgT_{<0.02\mu m}$ and $HgT_{<10\mu m}$ concentrations increased or remained at higher levels for Rep1 and Rep3. During t~~T~~his phase $P\text{-}HgT_{rel}$ vastly decreased ~~during~~ and was at a minimum of ~~xxx~~1-7 % by the end of the incubation. Contrastingly, $HgT_{<0.02\mu m}$ and $HgT_{<10\mu m}$ stayed constantly low for Rep2 during phase 3 and $P\text{-}HgT_{rel}$ remained overall above 50%. The Rep1 was the only MC that showed an increase in Cu concentrations during the draining phase (Fig. 4a).

In the HMLC +MNR MCs, pH remained in the range of 8 to 8.35 with minor fluctuations over both flooding periods (Fig. S7). ~~DOC concentrations were ranging between 72.2 and 134 mg L^{-1} (Fig. 2h). This was significantly higher (3 to 43 mg L^{-1}) than in HMLC control.~~The redox potential decreased rapidly from approx. E_h -300 mV to 5.27 ± 14.4 mV within the first 14 days and remained constant at 14.3 ± 8.12 mV during the second flooding period. Depletion of NO_3^- was observed within the first day of incubation and was under detection limit during the second flooding period (Fig. 2b). A rapid release of Mn started at day 2 and a slow release of Fe started at day 3 of first flooding period (Figs. 2c-f). The $[SO_4^{2-}]$:$[Cl^-]$ ratios decreased from 0.57 ± 0.01 to 0.37 ± 0.02 between day 4-29. During the

Formatted: Subscript
Formatted: Superscript
Formatted: Superscript
Formatted: Not Highlight
Formatted: Not Highlight
Formatted
Formatted: Not Highlight
Formatted: Not Highlight
Formatted: Not Highlight
Formatted: Not Highlight
Formatted: Not Highlight
Formatted: Not Highlight
Formatted: Not Highlight
Formatted: Subscript
Formatted: Not Superscript/ Subscript
Formatted: Highlight
Formatted: Subscript
Formatted: Superscript
Formatted: Superscript

second flooding period [SO_4^{2-}]:[Cl^-] ratios initially increased slightly between day 29-31 and then decreased to a minimum (0.12 ± 0.05) by the end of the incubation (Fig. 2g). DOC concentrations were ranging between 72.2 and 134 mg L^{-1} (Fig. 2h). This was significantly higher (3 to 43 mg L^{-1}) than in HMLC- without manure~~control~~. In these MCs $HgT_{<0.02\mu m}$ and $HgT_{<10\mu m}$ concentrations instantly increased together with the Mn release between days 0-4 (Phase 1) decreased during the days 5-14 (Phase 2) and remained low between day 14-42 (Phase 3) (Fig. 3 a-c). The particulate HgT (P-$HgT_{rel.}$) decreased to 30-52.5 % in phase 1 and remained overall above 50 % for the rest of the incubation. At the onset of phase 2 black precipitates were visually observed in the HMLC +MNR microcosms (Fig.S13). Cu concentrations decreased gradually during the course of the incubation experiment (Fig. 4a). Arsenic concentrations simultaneously increased with the release of Fe during the whole incubation (Fig. b).

LMHC differed from HMLC in soil solution chemistry. In both treatments (LMHC and LMHC +MNR), pH remained neutral but gradually decreased from 8.2 to 7.5 during the incubation (Fig. S7~~6~~). Soil reduction progressed rapidly from a max of 332 mV at day 3 to -14.3 mV at day 14 (Fig. ~~3~~5a~~f~~). During the second flooding E_h stayed in the range of - 2.3 to 34.5 mV. Nitrate was exhausted within the first day of incubation and marked the onset of Mn release. Mn as well as DOC concentrations gradually increased during the first flooding period (Fig. 5~~3~~b-c~~d~~-e). Fe release started on day 4 and day 6 in LMHC and LMHC +MNR respectively (Fig. 5d). A decrease in [SO_4^{2-}]:[Cl^-] ratio was observed after day 5 and remained stable at 0.03 ± 0.04 during the second flooding period. This is indicative for sulphate reduction during the draining phase and the second flooding phase (Fig. 5e). Soil solution $HgT_{<0.02\mu m}$ concentration (25 – 160 ng L^{-1}) were two orders of magnitude lower than in the HMLC runs (Fig2. 3a,6a). Dissolved $HgT_{<0.02\mu m}$ degreased during the first flooding period (phase 1), increased during the draining period (phase 2) and gradually decreased again during the second flooding period (phase 3) (Fig. 6a-c). No other soil solution parameter followed the trend of $HgT_{<0.02\mu m}$. Particulate $HgT_{<10\mu m}$ decreased during phase 1 and remained low during phase 2 and 3. In the LMHC MCs P-$HgT_{rel.}$ changed drastically between phase 1 (> 65 %) and phase 3 (<< 50 %) (Fig. 3c). In the LMHC +MNR MCs the P-$HgT_{rel.}$ was high during the phase 1 (> 65 %) and fluctuated between- phase 3 (<< 50 %) (Fig. 3c). Cu concentrations gradually decreased during the course of the experiment (Fig 7a). Arsenic concentrations simultaneously increased with the release of Fe during the whole incubation (Fig 7b).

~~3.1~~ 2 ~~Mercury dynamics (mobilization and sequestration).~~

~~In the HMLC control MCs, the pH of the soil solutions remained in a neutral to alkaline range of 8 to 8.4 throughout the whole experiment (Fig. S6). The DOC concentrations ranged between 37.5 and 106 mg L^{-1} (Fig. 2h). A continuous soil reduction was observed with completed NO_3^- reduction and the onset of Mn release at day 7 of the main incubation (Figs. 2d and S7). An increase of both $Hg_{<0.02\mu m}$ and $Hg_{<10\mu m}$ concentrations~~

~~the was simultaneous to the Mn release (Figs. 2a-e). Mean $Hg_{<0.02\mu m}$ concentration peaked on day 9 (17.1 ± 2.3 µg L^{-1} $Hg_{<0.02\mu m}$) and slightly decreased towards the end of the first flooding period on day 14 (13.7 ± 4.9 µg L^{-1} $Hg_{<0.02\mu m}$). The proportion of particulate Hg, $PHg_{rel.}$, gradually decreased from a maximum of 88 % to a minimum of~~

Formatted: Not Superscript/ Subscript

25 % at the end of the first flooding (Fig. 2e). $Cu_{<0.02\mu m}$ concentrations increased up to 88.2 ± 17.5µg L^{-1} within the first 4 days and then gradually decreased to 30.6 ± 3.54 µg L^{-1} at day 14 (Fig. 2e).

During the second flooding period, individual MCs behaved differently in the HMLC control treatment. The differences of soil solution E_h and redox sensitive trace metals (e.g. Cu, Mn, Hg, Fe, Cr) were apparent from the start of the second flooding (Figs. 2f-g, S8). Contrastingly, DOC concentrations and pH remained similar between incubators (Fig. 2h). Two replicates (Rep1; Rep3) showed a pronounced increase of E_h after the draining period (Fig. 2i). The Rep1 showed a depletion of Mn in soil solution indicating the formation of Mn oxide minerals but values obtained for $Hg_{<0.02\mu m}$ and $Mn_{<0.02\mu m}$ were then increased and peaked at 23.6 µg L^{-1} and 448 µg L^{-1} respectively during the second flooding. The $PHg_{rel.}$ decreased from 60 % to 30 %, and $Cu_{<0.02\mu m}$ concentrations were high (88.4 µg L^{-1}) at the onset but decreased to lower levels (11.8 µg L^{-1}). Further, the E_h of this MC remained high (150 to 300 mV) in this period. The E_h of Rep2 was lower (between 28 and 120 mV), Mn remained at the same level before and after draining phase, and no second release of Hg was observed. The Rep2 showed a release of Fe indicating the onset reduction of Fe oxyhydroxides, analogous to the Mn release in Rep1. The $PHg_{rel.}$ remained between 60 and 75 % in this MC. In Rep3, Mn remained at the same level before and after the draining period. During the second flooding, this MC showed a slightly lower release of Hg compared to Rep1, peaking at 10.9 µg L^{-1}, and associated to a decrease of $PHg_{rel.}$ from 60 % to 30 % and showed a faster decrease in DOC compared to the two other MCs (Fig. 2h).

In the cornfield soil MC with manure addition (HMLC +MNR) pH remained in the range of 8 to 8.35 with minor fluctuations throughout the experiment. DOC concentrations were ranging between 72.2 and 134 mg L^{-1} (Fig. 2h). This was significantly higher (3 to 43 mg L^{-1}) than in HMLC control. Soil solution redox potential decreased rapidly from approx. E_h 300 mV to 5.27 ± 14.4 mV within the first 14 days of the incubation in the HMLC +MNR treatment. It remained constant at 14.3 ± 8.12 mV during the second flooding period. Release of Mn and Hg started at day 2 of the main incubation once NO_3^- reduction was completed (Figs. 2, S6). Concentration of $Hg_{<0.02\mu m}$ peaked on day 4 at 15.9 ± 1.4 µg L^{-1}. By day 14, the Hg concentrations were close to the initial levels (1.73 ± 0.83 µg L^{-1} $Hg_{<0.02\mu m}$) and remained low the rest of the incubation experiment. The $PHg_{rel.}$ decreased to approx. 40 % during the release of Hg but was > 60 % before and after. With the onset of the decrease in soil solution Hg concentration, we visually observed black precipitates in the incubators with added manure. Unlike the HMLC control, MCs triplicates of HMLC +MNR behaved similarly during both flooding periods. No Hg release was observed during the second flooding.

LMHC differed from HMLC in soil solution Hg dynamics. In both treatments (LMHC and LMHC +MNR), pH remained neutral but gradually decreased from 8.2 to 7.5 during the incubation (Fig. S6). Soil reduction progressed rapidly from a max of 332 mV at day 3 to -14.3 mV at day 14 (Fig. 3f). During the second flooding E_h stayed in the range of - 2.3 to 34.5 mV. Mn as well as DOC concentrations gradually increased during the first flooding period (Fig. 3d-e). Soil solution $Hg_{<0.02\mu m}$ concentration (25 – 160 ng L^{-1}) are two orders of magnitude lower than in the HMLC runs (Fig. 3a). Both $Hg_{<0.02\mu m}$ and $Hg_{<10\mu m}$ decreased gradually during the first flooding period (Figs. 3a-b). No other soil solution parameter followed the trend of Hg. In both treatments but the $PHg_{rel.}$ differed clearly between first flooding (> 65 %) and second flooding period (<< 50 %) (Fig. 3c).

3.2 Colloidal Hg (AF4)

Hg bearing colloids were detected in all soil solution samples of HMLC incubations. Due to low signal to noise ratios (< 3) we did not detect colloidal Hg in samples of the LMHC incubations. Figure 8 shows the evolution of concentrations and relative proportions of HgT size fractions. Generally, changes in proportions were apparent during phases of Hg release and decrease in soil solution, but little change was observed during when Hg concentrations were stagnant (HMLC +MNR, Phase 3). The proportion of truly dissolved $HgT_{<1kDa}$ varied between 0 % and 67 % in the HMLC ~~control~~ experiment and was high during ~~the times of~~ Hg release to soil solution (phases 1 and 3) (Fig. 4~~8~~). In the HMLC +MNR treatment, $HgT_{<1kDa}$ were lower and ranged between 0 % and 29 %. The colloidal Hg can be divided into 3 main fractions (Fig. 9~~5~~). The first Hg colloidal fraction showed a main peak ranging between 1 – 40 kDa (d_h < 6 nm) and was associated with UV_{254nm}-absorbing compounds and various metals (Mn, Fe, Cu, Ni, Zn). This fraction was interpreted as humic substance type Hg–NOM. The proportion of this colloidal Hg fraction varied with no specific trends from 11.5 to 23.3 % in HMLC and 13.6 to 38.6 % in HMLC +MNR ~~though-out~~throughout the course of the experiment. A second fraction of Hg colloids ranged between 6 nm and 20 nm. This well-defined size fraction was eluting in the tail of the first fraction for other metals (e.g. Fe, Mn, Cu) but did not overlap with UV_{254nm} and fluorescence signals (Fig. ~~5~~9). This fraction could not be chemically defined but is hypothesized to consist of ß-$HgS_{(s)}$~~$HgS_{(s)}$~~ colloids. In the HMLC ~~control treatment~~run, we observed a decrease in the proportion of these inorganic colloids from 28 % ~~at the onset to~~in phase 0 to 15.3 % at the end ~~of the incubation~~ phase 3 (Fig. 4~~9~~). In the HMLC +MNR treatment, the proportion of this fraction ranged between 29.5 % and 41.9 % during the ~~first flooding~~phases 1 and 2 and could not be detected during the ~~second flooding~~ phase 3. Further, we observed a third colloidal fraction that continued to elute after the stop of the AF4 crossflow and it included colloids in the range of 30 – 450 nm (effective cut-off of the filter used for the sample preparation). In some cases, this fraction was better fitted using two overlapping populations (Fig. ~~5~~9, Figs. ~~S9~~S9-~~S12~~S12). In all the cases, HgT signal was associated with those of other metals and a slight bump of the UV_{254nm} signal but more specifically an increase of fluorescence signal associated to protein-like fluorophores. This fraction decreased continuously in the HMLC ~~control~~ runs ~~treatment~~ during the incubation from 32.4 % ~~at day 2~~ in phase 2 , to 5.6 % ~~at day 9~~ in phase 2 and stood under 9.1 % during ~~the rest of the incubation.~~phase 3. By contrast, the HMLC +MNR showed an increase in the proportion of this fraction from 7.3 % in phase 1 ~~at day 2~~ to 25.3 % by the end of ~~of the incubation~~phase 3 (Fig. 8~~4~~). The deconvolution of the fractograms included an intermediate fraction of Hg bearing colloids ranging between d_h = 6 nm and d_h = 450 nm depending on the sample. This fraction was added to refine the fractogram fittings but could not directly be associated to another measured metal. This indicates that this population represents~~overlap~~ a ~~more~~ polydispersed Hg particle population although in some cases the presence of small Hg particles dominates. This broad fraction was not detected in HMLC +MRN treatments during ~~the first flooding~~phases 1 and 2 but made up > 30 % during ~~the second flooding~~phase 3.

Formatted

3.3 ~~Net Hg methylation/demethylation~~ Net MeHg production in soil.

Soil MeHg levels fluctuated over the course of the incubation experiment (, Fig. 10~~6~~ and Table 2). Highest net MeHg production ~~net methylation was~~was observed during the first flooding period for the treatments with ma-

nureMNR (up to + 81 %) and during the draining phase for the treatments without MNR manure (up to + 73.1 %). We observed a significant decrease of MeHg/HgT and absolute MeHg concentrations in all incubators during the second flooding period (Fig. 106). In all MCs, MeHg/HgT increased by a factor of 1.18 to 1.36 throughout the incubation (Table 2).

4. Discussion

4.1 Mercury release and sequestration.

Cornfield soil (HMLC) and pasture field soil (LMHC) behaved very differently in this incubation experiment and will be discussed separately. In the cornfield soil (HMLC) Hg and Mn releases were simultaneous and started when soil solution E_h entered the field of Mn reduction below approx. 300mV (Figs. 2a, 2b2c,3a), strongly suggesting that this Hg pool was adsorbed to released by reductive dissolution of Mn-oxyhydroxides. The simultaneous decrease of the $PHg_{sol.}$ and $PMn_{sol.}$ indicates that Hg was adsorbed on both Mn-oxyhydroxides from soil and suspended particles (Figs. 2c and 2e). During all experiments, low Hg:DOM ratios (<<1 nmol Hg (mg DOM)$^{-1}$) suggest that strong binding sites of DOM were never saturated with respect to mercury, assuming a binding site [RS_2^{2-}] density of 5 nmol Hg (mg DOM)$^{-1}$ and that DOC is 50 % the DOM (Haitzer et al., 2002). The low Hg:DOM ratio suggests that Hg is mainly present as complexed with DOM given reported strong interaction with thiol sites of DOM. However, these assumptions might not reflect the actual composition of DOM which might drastically differ in amended soils (Li et al., 2019). Reductive dissolution of Mn-oxyhydroxides drives both 1.) the release of labile Hg-NOM complexes and Hg^{2+} sorbed on the oxide's surfaces and/or 2.) enhanced the degradation and mineralisation of unsubtle NOM binding Hg in soils (Jones et al., 2018). After Hg release (phase 1), Hg concentrations remained high and the relative particulate Hg fraction was low throughout the experiment. This illustrates that the released Hg-pool mainly originated from Mn-oxyhydroxides or degradation of suspended POM during Mn reduction. However, the released Hg-pool is relatively small compared the HgT levels of the soil. We estimate that about 12.8 ± 4.2 µg kg^{-1} Hg (0.02 % of HgT_{soil}) was evacuated by sampling during the experiment. The simultaneous decrease of the $PHg_{sol.}$ and $PMn_{sol.}$ indicates that Hg was adsorbed on both Mn-oxyhydroxides from soil and suspended particles (Figs. 2c and 2e). No other soil solution parameter (e.g. DOC) was directly related to the release of Hg. In In the fluvisol of our study areathis fluvisol, Hg mobilization is thus mainly not driven by the mobilization of DOM driven by reductive dissolution of Mn oxyhydroxides. Direct mobilization of DOM was reportet to govern Hg levels in unlike in peat soils, Histosols or Podsols in boreal environments environments (Åkerblom et al., 2008; Kronberg et al., 2016; Jiskra et al., 2017) or floodplain soils with higher OC levels (Beckers et al., 2019; Wang et al., 2021) in temperate soils. Further, Likewise we did not observe a mobilization of Hg mobilisation was not simultaneous to together with Cu release. This was as reported earlier for polluted soils with high Cu levels (Hofacker et al., 2013) and comparably low. This is explained by the comparably high Hg/Cu_{molar} ratio in the our soil matrix. After Hg release, Hg concentrations remained high and the particulate Hg fraction low throughout the experiment. This illustrates that the released pool of Hg mainly originated from Mn-oxyhydroxides and less from suspended POM nor particulate sulfide minerals in the cornfield soil. However, the pool bound to Mn-oxyhydroxides is relatively small. In neighbor-

Formatted: Not Highlight
Formatted: Not Superscript/ Subscript
Formatted: Not Highlight
Formatted: Superscript

~~in~~neighbouring soils, the main Hg pool was previously reported as $HgS_{(s)}$ and Hg complexed by recalcitrant NOM (Grigg et al., 2018). Earlier studies assumed that 0.1 to 0.6 % (w/w) of NOM was reduced sulphur with high affinity to Hg (Grigg et al., 2018; Ravichandran, 2004). Following this assumption, reduced ~~sulfur~~sulphur groups of the cornfield soils NOM could sorb between 11.9 to 71.9 mg kg^{-1} of Hg. The soils high Hg concentration (474.3 ± 0.58 mg ~~L~~kg^{-1}) suggests, that soil NOM thiol sites are likely saturated in terms of Hg. Therefore, saturated NOM sorption sites are not competing with Mn-oxyhydroxide sorption sites, resulting in a substantial Mn-oxyhydroxide bound Hg-pool. This leads to a higher mobility of Hg upon reductive dissolution of Mn-oxyhydroxide compared to fluvisols used in other incubation studies (Hofacker et al., 2013; Poulin et al., 2016; Beckers et al., 2019).

During the second flooding phase, the cornfield soil (-HMLC) ~~control~~ runs showed a higher variability in redox sensitive soil solution parameters (Fig. 2). This might be explained as 1~~a~~.) a shift in microbial communities, 2~~b~~.) disturbance of the soil column by invasive soil sampling in between the flooding periods or 3~~c~~.) uneven draining of the pore space after the first flooding. It can also reflect how redox cycle can be easily affected *in situ*. We suggest that the second release of Mn and Hg in Rep1 is due to Mn re-oxidation during the draining period and a second reductive dissolution of Mn oxyhydroxides upon reflooding. This is supported by the elevated E_h at the onset of the second flooding.~~-~~ ~~Further, Mn reduction oxidation and reduction cycles were shown to enhance the degradation of NOM to more labile forms~~ (Jones et al., 2018) ~~which might contribute to the degradation/mineralization of recalcitrant Hg-NOM.~~ ~~This is supported by the elevated E_h at the onset of the second flooding.~~ The HMLC ~~control~~ Rep3 showed a second release of Hg without a remobilization of Mn. Changing redox conditions have been shown to enhance microbial respiration and therefore NOM degradation (Sunda and Kieber, 1994). ~~Further, Mn oxidation was shown to enhance the degradation of larger NOM to LMW NOM (Jones et al., 2018).~~ Thus, we interpret the second Hg release in Rep 3 as a degradation/mineralization of NOM that bound Hg.

The carbon amendments were reported to decrease total Hg release in polluted floodplain soils (Beckers et al., 2019) but may have a mobilizing effect in NOM depleted environments (Eckley et al., 2021). The addition of manure accelerated the release of Hg through reductive dissolution of Mn oxyhydroxides in the cornfield soil (HMLC). Mercury was released 4 day earlier ~~in the +MNR group compared to the control. . We interpret this~~ as ~~an effect~~result of additional ~~organic~~ labile carbon of the liquid manure 1.) acting as electron donor enhancing microbial ~~activity~~soil reduction (Liu et al., 2020), 2.) act directly as reductant of the Mn oxyhydroxides (Remucal and Ginder-Vogel, 2014). In the manure treatment, we observed a fast decrease of Hg concentration and a constantly high proportion of particulate P-$Hg_{T_{rel,0.02\mu m,10\mu m}}$ even after the plateau of Mn concentration in soil solution and the relative decrease of particulate Mn. The addition of manure ~~represents an addition of 0.3 g of fresh NOM to the MCs. It is~~ a source of POM (manure was sieved to < 500 µm) and increased DOC approximately by 20 mg L^{-1}. Sorption of Hg is directed towards thiol rich high molecular weight NOM (Liang et al., 2019) following different ligand exchange reactions (e.g. carboxyl-groups to thiol groups) which happen within days (Miller et al., 2009; Chiasson-Gould et al., 2014). ~~Therefore, w~~The constant of P-Hg_{rel} ~~e explain the decrease of Hg by a continuous~~proportion is suggested to be partly caused~~-~~ by the complexation of dissolved ~~mobilized~~ Hg with the added ~~NOM~~ POM of the manure.

~~The freshly added manure served as a source of new thiol sites. Adsorption of Hg is directed towards larger more thiol rich NOM (Liang et al., 2019) and different ligand exchange reactions (e.g. carboxyl-groups to thiol groups)~~

Formatted: Not Superscript/ Subscript

Formatted: Subscript

~~happen within days (Miller et al., 2009; Chiasson-Gould et al., 2014).~~ In addition, we visually observed black precipitates (Fig. S13)~~d at the first day of Hg decrease in the MCs with manure addition (Fig. S13)~~and the decrease of $[SO_4^{2-}]$:$[Cl^-]$ ratios (Fig. 2g) at the onset of Hg decrease (phase 2) in the MCs with manure addition. This ~~indicat~~indicates~~ing~~ the precipitation of ~~sulfi~~sulphide mineral particles. ~~-~~ Although, ~~Although, E_h~~redox potential measurements did not indicate sulphate reduction, the monitoring of E_h in soil solution provides only a qualitative measure in a complex soil systems. ~~, the formation of sulfide minerals in micro- and meso-pores are possible. Furthermore, the formation of $HgS_{(s)}$ from Hg-NOM was reported even under oxic conditions~~ (Manceau et al., 2015).~~We suggest that, formation and aggregation of $HgS_{(s)}$ explains the faster decrease in the manure amended experiment. Furthermore, formation of metacinnabar ß-$HgS_{(s)}$ was observed under oxic conditions by conversion of thiol bound $Hg(SR)_2$ (Manceau et al., 2015). ~~-~~The formation and aggregation of $HgS_{(s)}$ is further supported by AF4 results (Sect. 4.2). ~~In both scenarios the addition of manure would accelerate the process either by promoting soil reduction or as additional source of NOM.~~

Hofacker et al., 2013~~-Hofacker et al. (2013)~~ reported a quantitatively relevant incorporation of Hg into metallic Cu^0 particles. However, we do not consider this a relevant pathway, due to the relatively high Hg/Cu_{molar} ratio in our soil compared to~~-~~Hofacker et al., 2013 Hofacker et al. (2013). Although the simultaneous decrease of Hg and Cu may be interpreted as the immobilization of Hg though incorporation into metallic Cu particles, i) we did not observe the formation of colloidal Cu associated with Hg (Sect. 6.2) and ii) relatively high Hg/Cu molar ratios indicate that the decrease of Hg in the soil solution cannot be solely explained by this mechanism as Hg would be marginally incorporated metallic Cu^0 particles.

As well, Hg in soil solutions ~~may be~~is volatilized by reduction of Hg^{2+} to Hg^0 (Hindersmann et al., 2014; Poulin et al., 2016). Our experimental design did not allow for quantification of gaseous Hg^0 and it may have exited the MCs since they were only sealed with parafilm. Reduction of Hg^{2+} may happen both biotically (Grégoire and Poulain, 2018) and abiotically under UV-light and in the dark (Allard and Arsenie, 1991). ~~The former process~~Biotic reduction is a detoxication mechanism of bacteria carrying *merA* genes in Hg polluted environments. Biotic volatilization has been observed in neighboring soils of our sampling site (Frossard et al., 2018). Organic amendments and high Hg levels have been shown to increase the abundance of Hg reducing bacteria (Hu et al., 2019). Further, dark abiotic reduction of Hg^{2+} complexed to functional groups of DOM in soils has been demonstrated (Jiang et al., 2015). However, it is unlikely that Hg reduction can solely explain the decrease of Hg in the soil solution in our microcosms. We therefore interpret the decrease in Hg concentration to be due to a combination of manure NOM complexation and sequestration together with the formation of $HgS_{(s)}$ during flooding. Our data shows that manure addition may have an immobilizing effect on Hg in flooded soils. By contrast, carbon amendments may increase Hg mobility and methylation in NOM depleted and cinnabar rich mountain soils (Eckley et al., 2021).

In the pasture field soil (LMHC), soil solution Hg concentrations remained at low levels (< 0.16 µg L^{-1} $Hg_{<0.02µm}$) during the whole experiment in both treatments (Fig. ~~3a~~6a). Unlike in the cornfield soil (HMLC), we did not observe a simultaneous release of Hg upon Mn reduction (Fig. ~~3d~~5c). We explain this with the not completely Hg saturated NOM in this soil, if we assume that 0.1 – 0.6 % (w/w) of NOM was reduced S with high affinity to Hg (Grigg et al.,

Formatted: Subscript
Formatted: Superscript
Formatted: Superscript
Formatted: Subscript
Field Code Changed
Field Code Changed
Formatted: Superscript
Formatted

2018; Ravichandran, 2004; Skyllberg, 2008). Thus, the pasture field soil has a rather limited pool of labile Hg compared to the cornfield soil. Both $Hg_{<0.02\mu m}$ and $Hg_{<10\mu m}$ negatively correlate with the sum of sampled soil solution (R^2 = -0.841, p= <0.001) during both flooding periods and. ~~Both $Hg_{<0.02\mu m}$ and $Hg_{<10\mu m}$ pools decreased~~ fastly decreased. This suggests that ~~a~~ the concentration gradient between supernatant artificial rainwater and the soil solution contributed to the fast exhaustion of the small labile Hg pool in pasture field soil. The presence of this concentration gradient in our incubation setup is confirmed by the continuously decreasing concentrations of conservative ions (Cl^-, Na^+, K^+) in soil solutions of the HMLC runs (Sect. S5.2, Figs. ~~S6~~S7, ~~S7~~S8). The relatively high proportion of particulate Hg vastly decreased during the draining period (Fig. 3b,c) and we speculate that this change is a result of the mobilization of the POM–Hg pool by mineralization/degradation of NOM which sorbed Hg during the draining period (Jones et al., 2018). In summary, flooding of the pasture field soils did mobilize only a small pool of particulate bound Hg which was exhausted within the first flooding period.

4.2 Colloidal Hg

~~In the absence of~~For runs without manure, AF4 results show that the Hg released from Mn-oxyhydroxides (Sect. 6.1.2) was dominated by truly dissolved Hg (Hg^{2+} or LMW–NOM–Hg) (Fig. 4~~8~~). The high Cl^- concentrations (up to 800 mg L^{-1}, Fig. ~~S14~~S14) likely influenced the Hg speciation in the soil solution, as chloride is a main complexant for Hg^{2+} (Li et al., 2020; Gilli et al., 2018). During Hg release, the proportions of larger Hg colloids (> 25 nm) decreased. The stable proportion of humic substances bound Hg and inorganic Hg colloids between 6 nm and 25 nm indicates that once released no major adsorption or aggregation of truly dissolved Hg and larger colloidal Hg occurs. Additional complexation of Hg by DOM can be excluded if we assume the saturation state of thiol-sites of the NOM pool in the soil (Sect. 6.1.2). These observations illustrates the remarkably high Hg mobility and potentially increased bioavailability (proportion of truly dissolved Hg) to Hg metabolizing microorganisms compared to other studies (Hofacker et al., 2013; Poulin et al., 2016). These authors did either not observe Hg in truly dissolved form or a decrease~~d~~ to low levels within the first days of incubation. Overall, the released Hg from cornfield soil (HMLC) shows a high mobility and might represent a possible threat to downstream ecosystems and a source for Hg methylating bacteria. However, the ~~released~~ total Hg released and sampled from ~~soil matrix~~ soil solution represents a rather small pool (12.8 ± 4.2 µg HgT kg^{-1} soil) of the total Hg (47.3 ± 0.5 ~~44.8~~ mg kg^{-1}). Further work would be needed to establish a Hg flux model to better understand *in situ* soil Hg mobility in these soils.

Formatted: Superscript

The manure addition had a key effect on the proportions of colloidal fractions in soil solution, and overall led to a low proportion of truly dissolved fraction (Fig. 4~~8~~). We suggest that the distinct fraction of colloids with d_h = 6 – 25 nm represents metacinnabar like $HgS_{(s)}$ colloids (Gerbig et al., 2011). This is supported by the onset of sulphate reduction in phase 2 (Rivera et al., 2019) and reported Hg-NOM interactions that may cause of may cause the precipitation of Hg bearing sulphide phases ($FeS_{(s)}$, ß-$HgS_{(s)}$) (Manceau et al., 2015) (Sect. 6.1.1). The size of ß-$HgS_{(s)}$ nano particles formed from free sulphide is dependent in the sulphide concentration as well as on the Hg:DOM ratio (Poulin et al., 2017). The formation of a distinct size fraction of HgS(s) has experimentally observed at comparable Hg:DOM ratios (Gerbig et al., 2011). The Hg colloidal distribution was dominated by the presence of large fractions (d_h = 30 - 450 nm). Larger organic acids with high aromaticity usually contain higher proportions of thiols groups

than smaller molecules and selectively complex Hg (Haitzer et al., 2002). This suggests that Hg complexation is kinetically driven and it can shifts from LMW–DOM to larger NOM and larger aggregates of POM as supported by earlier incubation experiments (Poulin et al., 2016). We therefore interpret that the relative increase of Hg colloids with d_h = 30 – 450 nm (Fig. 48) is caused ~~as a~~ by 1.) complexation of the released dissolved $Hg_{<1kDa}$ by ~~thiol groups~~ strong binding sites of thiol rich~~of~~ NOM in larger clay-organo-metal complexes and 2.) the aggregation of $HgS_{(s)}$ colloids ~~during the experiment~~. Although

~~The onset of sulfate reduction (Rivera et al., 2019) as well as the interaction of Hg with NOM (Manceau et al., 2015) may cause the precipitation of Hg bearing sulfide minerals and nanoparticles ($FeS_{(s)}$, ß-$HgS_{(s)}$) (Sect. 6.1.1). We therefore suggest that the distinct fraction of colloids with d_h = 6 – 25 nm is $HgS_{(s)}$. The AF4 fractograms show the presence of these colloids during the first flooding period but not during the second flooding one. Moreover, the proportion of the intermediate fraction increased in the second flooding. Although~~ the presence of e.g. humic substances and larger NOM was shown to narrow the size range of $HgS_{(s)}$ nanoparticles precipitating from solution (Aiken et al., 2011) , through time, these colloids may grow, aggregate and form clusters in a wide size distribution (Deonarine and Hsu-Kim, 2009; Poulin et al., 2017). Thus, their aggregation during the draining period may explain ~~We explain the~~the decrease in ~~disappearance of~~ monodisperse Hg bearing colloids ~~by their aggregation during the draining period~~, also leading ~~also~~ to sequestration of Hg in the soil matrix, without remobilization during the second flooding. Our data suggests meta cinnabar formation (ß-$HgS_{(s)}$) in a distinct size fraction (d_h = 6 – 25) and their aggregation to large fractions (d_h = 30 – 450 nm) at environmental conditions in real-world samples.

4.3 Net MeHg production ~~Net methylation~~ in soil ~~during flooding draining experiment~~.

The studied soils show uncommonly high initial MeHg levels (6.4 – 26.9 µg kg^{-1}) when compared to other highly polluted mining or industrial legacy sites (Horvat et al., 2003; Neculita et al., 2005; Qiu et al., 2005; Fernández-Martínez et al., 2015). ~~. The soils were~~ supposedly as a result of a flooding event~~ed~~ prior to sampling resulting in a net MeHg production ~~in the methylation of MeHg before the field sampling~~. Still, we observed significant net MeHg production ~~MeHg production~~ during the first 28 days of the incubation resulting in even higher MeHg concentrations of up to 44.81 µg kg^{-1} (Table 3; Fig. ~~6~~10). Soils treated with manure showed a faster net MeHg production ~~methylation~~ with highest ~~net~~ increase of ~~methylation~~ MeHg during the first flooding period. Controls showed highest ~~net~~ net MeHg production ~~methylation~~ during the draining period and reached similar levels of MeHg at the start of the second flooding on day 28 (Fig. ~~6~~10). For cornfield soil (HMLC), both treatments show a high concentration ~~of highly bioavailable~~ of bioavailable Hg^{2+} or Hg associated with labile NOM ($HgT_{<0.02µm}$ > 15µg L^{-1} ~~and $Hg_{<1kDa}$~~) in soil solution during the first flooding ~~(add publication)~~. Net MeHg production ~~Methylation~~ is therefore rather limited by cellular uptake of Hg or the microbial activity of methylating microorganisms than bioavailability. Thus, we interpreted the addition of labile carbon in the form of manure to result in a higher microbial activity and net MeHg production ~~higher MeHg~~ during the first flooding period. However, we did neither assess the activity nor the abundance of Hg methylating bacteria such as sulphate reducers (SRB), Fe reducers (FeRB), archaea or firmicutes (Gilmour et al., 2013). In the ~~control~~ runs without manure addition, a substantial part of Hg was methylated during the draining period. This indicates that even if low concentrations of Hg is released (LMHC MCs day 14:

Formatted: Subscript

Formatted: Not Superscript/ Subscript

Formatted: English (United States)

Formatted: Superscript

Formatted: Superscript

HgT$_{<0.02\mu m}$ < 50 ng L^{-1}) a substantial amount of Hg can be methylated. Micro- and meso pore spaces with steep redox gradients act as ideal environments for microbial methylation even in drained and generally aerobic system (e.g. HMLC without manure ~~control~~ during the draining period).

Further, we observed a decrease in ~~net demethylation~~absolute MeHg concentrations in all MCs during the second flooding period. Oscillating net de-/methylation in environments characterized by flood-drought-flood cycles have been reported earlier (Marvin-DiPasquale et al., 2014). Degradation of MeHg was reported to happen either abiotically by photodegradation or biotically by chemotrophic reductive or oxidative demethylation by microorganisms carrying the *mer*-operon (Grégoire and Poulain, 2018). ~~A p~~Photodegradation of MeHg can be excluded as the experiment was conducted in the dark. However, demethylation could have happened as biotic reductive demethylation. A possible explanation is a MeHg detoxification reaction by microorganisms carrying the *mer*-operon (*merB*) (Hu et al., 2019; Frossard et al., 2018; Dash and Das, 2012). However, we can only hypothesize about demethylation mechanisms, as neither communities (DNA) nor gene expression (mRNA)~~s~~ dynamics in the soils were ~~analyzed~~analysed during the experiment.

4.4 Experimental Limitations

Incubation experiments on a laboratory scale are a common way to study the changes in mobility of trace elements in floodplain soils (Gilli et al., 2018; Frohne et al., 2011; Poulin et al., 2016; Abgottspon et al., 2015). These study designs allow for controlled conditions and replicable results. However, controlled experiments usually fail to cover the complexity of a real floodplain soil system (Ponting et al., 2020). Our study design did not involve temperature gradients, realistic hydrological flow conditions or intact soil structure. In this study, the artificial rainwater and the soil were equilibrated by shaking for a few minutes. However, the equilibration appeared to be incomplete with respect to highly soluble chloride bearing minerals for the experiment with cornfield soil (Fig. ~~S14~~S14). ~~This is supported~~The incomplete equilibration is indicated by the temporal patterns of conservative ions (Cl^-, K^+ and Na^+) in soil solution (Figs. ~~S6~~S7, ~~S7~~S8) and the difference in Cl^- concentration between the soil solutions at t = 6 h and the same water-soil mixture shaken for 6 h (Fig. ~~S14~~S14). These patterns are a result of a concentration gradient between supernatant water and the solution in the soil pore space. They ~~These patterns were~~ only became visible, due to high levels of conservative ions ~~these elements~~ to start with, which most likely stem ~~form~~ from a fertilisation event ~~that must have taken place just~~ prior to sampling the soil. ~~Nonetheless, they~~ Infiltration of supernatant water was facilitated by the sampling of 4-6 % of the total added water at each time point. This resulted in a~~how that soil solution sampling removed a considerable amount of dissolved elements~~The infiltration of surface water further led to a dilution of the soil solution~~.~~. Consequently, the continuous decrease in sulphate was not directly indicative for sulphate reduction, but the result of this dilution effect. ~~and the decrease in soil solution concentration of some elements can be linked to the sampling, making their interpretation difficult. The infiltration of surface water further led to a dilution of the soil solution.~~ However, this effect did not directly affect the the release of soil bound elements (e.g. ~~As,~~ Hg, Mn, Fe, Assss) by e.g. reductive dissolution~~, do not seem to be directly affected by this mechanism~~ (Figs. 2,3,4). It should also be noted that high initial Cl^- concentrations in the soil solution, may influence Hg

Field Code Changed

solubility since Cl^- is a complexant for Hg^{2+} (Li et al., 2020) and this warrants further studies on the role of inorganic fertilisation on Hg mobility.

5. Conclusions

We studied the effect of manure addition on the mobility of Hg in soil during a flooding-draining experiment. ~~Further, we~~ We observed ~~the~~ formation and size distribution changes of Hg colloids (ß-$HgS_{(s)}$, Hg-NOM) at environmental conditions ~~of Hg colloids~~ in soil solution by AF4–ICP–MS.~~,~~ The results of this study show that manure addition ~~has a distinct effect on~~ 1.) ~~temporal Hg release and sequestration~~diminished HgT mobility, 2.) facilitated Hg complexation with fresh NOM and ~~colloid~~ formation of ß-$HgS_{(s)}$ and 3.) had only limited effect on ~~net methylation~~ net MeHg production ~~dynamics~~ in polluted and periodically flooded soils.

~~In the cornfield soil (HMLC), Hg~~Mercury was mobilized upon reductive dissolution of Mn oxy~~-~~hydroxides in highly Hg polluted (47.3 ± 0.5 mg kg^{-1}) and NOM poor soils. The application of manure accelerated the release of Hg, facilitated the formation of colloidal Hg and exhausted the mobile Hg pool within the first 7 days of flooding. This prevented Hg remobilization during the second flooding period. Contrastingly, ~~In pasture field (LMHC) soil~~ Hg was mainly released as particulate bound Hg ~~presumably due to the higher soil organic carbon content~~in soils with moderate Hg pollution (2.4 ± 0.3 mg kg^{-1}) and high NOM levels. Ppresumably, due to its higher soil organic carbon content. This relatively small pool of particulate Hg was exhausted within the first flooding period. In both soils, soil reduction enhanced net MeHg production of a substantial part of the Hg pool as confirmed by MeHg formation upon flooding-draining cycles ~~suggest that the changes of redox conditions enhance methylation of a substantial part of the Hg pool~~. However, ~~However,~~ MeHg was either subsequently ~~declines~~ removed from the ~~from the~~ soil by ~~either~~ advective transport of dissolved MeHg in the soil column or transformed by reductive demethylation. ~~Due to the wide differences in bioavailable Hg between treatments and soils w~~We suggest that the temporal changes in net MeHg production~~net methylation~~ are limited by microbial activity of Hg methylators, given the similar net MeHg production in treatments and soils with variable dissolved Hg levels. Microbial ~~Their~~ activity ~~appears~~ is likely to be stimulated ~~facilitated~~ by ~~fresh~~ manure addition.

The release of Hg from polluted soils to downstream ecosystems does depend on both biogeochemical conditions as well as on hydrological transport. Our experiment shows that redox oscillations (flooding-draining-flooding cycles) of a polluted floodplain soil are likely to induce pulses of both Hg and MeHg to the downstream ecosystems. This is supported with earlier studies (Poulin et al., 2016; Frohne et al., 2012; Hofacker et al., 2013). In contrast to NOM rich soil systems, we show that the Mn dynamics may govern the release of Hg in highly polluted soil systems low in NOM. ~~In NOM poor agricultural soils, the application of additional NOM in form of manure may reduce the mobilization and contribute to the transformation of Hg towards less mobile species, especially during low flow conditions.~~Further, the application of additional NOM in form of manure facilitates soil reduction, contributed to the transformation of Hg towards less mobile species reduced the Hg mobilization. ~~With respect to Hg mobiliy~~However, effects of carbon amendments (organic amendments or biochar) are contrasting between enhancing (Li et al., 2019; Eckley et al., 2021) and diminishing (Beckers et al., 2019; Wang et al., 2020; Wang et al., 2021) Hg mobility.~~.~~ We therefor ~~emphasize~~stress the need ~~of~~ for characterisation of soil properties and especially NOM in future stud~~ie~~ies

Formatted: Not Superscript/ Subscript

focusing on Hg mobility upon ~~y~~organic amendments (Li et al., 2019)~~.~~ ~~Overall, more work is~~We further emphasize the need of ~~needed to understand the mobilization of Hg in polluted areas. More precisely,~~ field trials integrating biogeochemical processes, hydrological transport and Hg soil-air exchange ~~are needed~~ in order to establish Hg flux models to better understand *in situ* soil Hg mobility.

Formatted: Normal

Data availability.

Details of analytical methods, AF4–ICP–MS fractograms are given in the Supplement. A complete dataset of the data used in this study is accessible at ~~http://doi.org/10.5281/zenodo.4058676~~http://doi.org/10.5281/zenodo.4715110 ~~10.5281/zenodo.4058676~~

Formatted: Default Paragraph Font

Acknowledgements.

We acknowledge P. Neuhaus, J. Caplette, K. Trindade, K. Kavanagh, and D. Fischer for the help in the laboratory. We thank T. Erhardt at the Climate and Environmental Physics (CEP) at University of Bern for the ICP–TOF–MS analyses and~~.~~ ~~Stefan~~ Stephane Westermann at the Dienststelle für Umweltschutz (DUS) of the Canton Wallis for the help with site selection and sampling permissions. Soil temperatures have been provided by MeteoSwiss, the Swiss Federal Office of Meteorology and Climatology. Klaus Jarosch and Moritz Bigalke of the soil science group at the Institute of Geography at University of Bern gave valuable ~~for the~~ advice ~~advises~~ during the writing process.

Author contribution.

AM and LG designed the study. LG and AW preformed the incubation experiments. LG and IW performed laboratory analyses. LG and IW performed the data analysis. AM and VS supervised and financed the study. LG prepared the manuscript with contributions from all co-authors.

Financial support.

This work was funded the Swiss National Science Foundation (SNSF, Nr. 163661). VS and IW acknowledge the financial support of the SNSF R'Equip project Nr. 183292.

Review statement.

References

Abgottspon, F., Bigalke, M., and Wilcke, W.: Fast colloidal and dissolved release of trace elements in a carbonatic soil after experimental flooding, Geoderma, 259-260, 156–163, doi:10.1016/j.geoderma.2015.06.005, 2015.

706 Aiken, G. R., Hsu-Kim, H., and Ryan, J. N.: Influence of dissolved organic matter on the environmental fate of
707 metals, nanoparticles, and colloids, Environmental science & technology, 45, 3196–3201,
708 doi:10.1021/es103992s, 2011.
709 Åkerblom, S., Meili, M., Bringmark, L., Johansson, K., Kleja, D. B., and Bergkvist, B.: Partitioning of Hg Between
710 Solid and Dissolved Organic Matter in the Humus Layer of Boreal Forests, Water Air Soil Pollut, 189, 239–252,
711 doi:10.1007/s11270-007-9571-1, 2008.
712 Allard, B. and Arsenie, I.: Abiotic reduction of mercury by humic substances in aquatic system.: An important pro-
713 cess for the mercury cycle, Water Air Soil Pollut, 457–464, 1991.
714 AMAP/UN Environment: Technical Background Report for the Global Mercury Assessment 2018, Arctic Monitor-
715 ing and Assessment Programme, Oslo, Norway/UN Environment Programme, Chemicals and Health Branch,
716 Geneva, Switzerland, Geneva, Switzerland, 426 pp., 2019.
717 Amos, H. M., Jacob, D. J., Streets, D. G., and Sunderland, E. M.: Legacy impacts of all-time anthropogenic emis-
718 sions on the global mercury cycle, Global Biogeochem. Cycles, 27, 410–421, doi:10.1002/gbc.20040, 2013.
719 Beckers, F., Mothes, S., Abrigata, J., Zhao, J., Gao, Y., and Rinklebe, J.: Mobilization of mercury species under
720 dynamic laboratory redox conditions in a contaminated floodplain soil as affected by biochar and sugar beet fac-
721 tory lime, The Science of the total environment, 672, 604–617, doi:10.1016/j.scitotenv.2019.03.401, 2019.
722 Beckers, F. and Rinklebe, J.: Cycling of mercury in the environment: Sources, fate, and human health implications:
723 A review, Critical Reviews in Environmental Science and Technology, 23, 1–102,
724 doi:10.1080/10643389.2017.1326277, 2017.
725 Biester, H., Müller, G., and Schöler, H.: Binding and mobility of mercury in soils contaminated by emissions from
726 chlor-alkali plants, Science of The Total Environment, 284, 191–203, doi:10.1016/S0048-9697(01)00885-3,
727 2002.
728 Bigham, G. N., Murray, K. J., Masue-Slowey, Y., and Henry, E. A.: Biogeochemical controls on methylmercury in
729 soils and sediments: Implications for site management, Integrated environmental assessment and management,
730 13, 249–263, doi:10.1002/ieam.1822, 2017.
731 Bravo, A. G., Bouchet, S., Tolu, J., Björn, E., Mateos-Rivera, A., and Bertilsson, S.: Molecular composition of or-
732 ganic matter controls methylmercury formation in boreal lakes, Nature communications, 8, 14255,
733 doi:10.1038/ncomms14255, 2017.
734 Chiasson-Gould, S. A., Blais, J. M., and Poulain, A. J.: Dissolved organic matter kinetically controls mercury bioa-
735 vailability to bacteria, Environmental science & technology, 48, 3153–3161, doi:10.1021/es4038484, 2014.
736 Deonarine, A. and Hsu-Kim, H.: Precipitation of Mercuric Sulfide Nanoparticles in NOM-Containing Water: Impli-
737 cations for the Natural Environment, Environ. Sci. Technol., 43, 2368–2373, doi:10.1021/es803130h, 2009.
738 Deonarine, A., Lau, B. L. T., Aiken, G. R., Ryan, J. N., and Hsu-Kim, H.: Effects of humic substances on precipita-
739 tion and aggregation of zinc sulfide nanoparticles, Environmental science & technology, 45, 3217–3223,
740 doi:10.1021/es1029798, 2011.
741 Driscoll, C. T., Mason, R. P., Chan, H. M., Jacob, D. J., and Pirrone, N.: Mercury as a global pollutant: Sources,
742 pathways, and effects, Environmental science & technology, 47, 4967–4983, doi:10.1021/es305071v, 2013.

743 Drott, A., Lambertsson, L., Björn, E., and Skyllberg, U.: Importance of Dissolved Neutral Mercury Sulfides for
744 Methyl Mercury Production in Contaminated Sediments, Environ. Sci. Technol., 41, 2270–2276,
745 doi:10.1021/es061724z, 2007.
746 Dublet, G., Worms, I., Frutschi, M., Brown, A., Zünd, G. C., Bartova, B., Slaveykova, V. I., and Bernier-Latmani,
747 R.: Colloidal Size and Redox State of Uranium Species in the Porewater of a Pristine Mountain Wetland, Envi-
748 ronmental science & technology, 53, 9361–9369, doi:10.1021/acs.est.9b01417, 2019.
749 Eckley, C. S., Luxton, T. P., Stanfield, B., Baldwin, A., Holloway, J., McKernan, J., and Johnson, M. G.: Effect of
750 organic matter concentration and characteristics on mercury mobilization and methylmercury production at an
751 abandoned mine site, Environmental pollution (Barking, Essex 1987), 271, 116369,
752 doi:10.1016/j.envpol.2020.116369, 2021.
753 Eklöf, K., Bishop, K., Bertilsson, S., Björn, E., Buck, M., Skyllberg, U., Osman, O. A., Kronberg, R.-M., and Bravo,
754 A. G.: Formation of mercury methylation hotspots as a consequence of forestry operations, The Science of the
755 total environment, 613-614, 1069–1078, doi:10.1016/j.scitotenv.2017.09.151, 2018.
756 Fernández-Martínez, R., Larios, R., Gómez-Pinilla, I., Gómez-Mancebo, B., López-Andrés, S., Loredo, J., Ordóñez,
757 A., and Rucandio, I.: Mercury accumulation and speciation in plants and soils from abandoned cinnabar mines,
758 Geoderma, 253-254, 30–38, doi:10.1016/j.geoderma.2015.04.005, 2015.
759 Frohne, T., Rinklebe, J., Diaz-Bone, R. A., and Du Laing, G.: Controlled variation of redox conditions in a flood-
760 plain soil: Impact on metal mobilization and biomethylation of arsenic and antimony, Geoderma, 160, 414–424,
761 doi:10.1016/j.geoderma.2010.10.012, 2011.
762 Frohne, T., Rinklebe, J., Langer, U., Du Laing, G., Mothes, S., and Wennrich, R.: Biogeochemical factors affecting
763 mercury methylation rate in two contaminated floodplain soils, Biogeosciences, 9, 493–507, doi:10.5194/bg-9-
764 493-2012, 2012.
765 Frossard, A., Donhauser, J., Mestrot, A., Gygax, S., Bååth, E., and Frey, B.: Long- and short-term effects of mercury
766 pollution on the soil microbiome, Soil Biology and Biochemistry, 120, 191–199,
767 doi:10.1016/j.soilbio.2018.01.028, 2018.
768 Gerbig, C. A., Kim, C. S., Stegemeier, J. P., Ryan, J. N., and Aiken, G. R.: Formation of nanocolloidal metacinnabar
769 in mercury-DOM-sulfide systems, Environmental science & technology, 45, 9180–9187,
770 doi:10.1021/es201837h, 2011.
771 Gilli, R., Karlen, C., Weber, M., Rüegg, J., Barmettler, K., Biester, H., Boivin, P., and Kretzschmar, R.: Speciation
772 and Mobility of Mercury in Soils Contaminated by Legacy Emissions from a Chemical Factory in the Rhône
773 Valley in Canton of Valais, Switzerland, Soil Syst., 2, 44, doi:10.3390/soilsystems2030044, 2018.
774 Gilmour, C. C., Podar, M., Bullock, A. L., Graham, A. M., Brown, S. D., Somenahally, A. C., Johs, A., Hurt, R. A.,
775 Bailey, K. L., and Elias, D. A.: Mercury methylation by novel microorganisms from new environments, Envi-
776 ronmental science & technology, 47, 11810–11820, doi:10.1021/es403075t, 2013.
777 Glenz, C. and Escher, J.-R.: Voruntersuchung von belasteten Standorten: Historische Untersuchung Objekt
778 Grossgrundkanal, FUAG-Forum Umwelt AG, Visp, Switzerland, 89 pp., 2011.

Formatted: German (Switzerland)

779 Graham, A. M., Aiken, G. R., and Gilmour, C. C.: Dissolved organic matter enhances microbial mercury methyla-
780 tion under sulfidic conditions, Environmental science & technology, 46, 2715–2723, doi:10.1021/es203658f,
781 2012.
782 Graham, A. M., Aiken, G. R., and Gilmour, C. C.: Effect of dissolved organic matter source and character on micro-
783 bial Hg methylation in Hg-S-DOM solutions, Environmental science & technology, 47, 5746–5754,
784 doi:10.1021/es400414a, 2013.
785 Grégoire, D. S. and Poulain, A. J.: Shining light on recent advances in microbial mercury cycling, FACETS, 3, 858–
786 879, doi:10.1139/facets-2018-0015, 2018.
787 Grigg, A. R. C., Kretzschmar, R., Gilli, R. S., and Wiederhold, J. G.: Mercury isotope signatures of digests and
788 sequential extracts from industrially contaminated soils and sediments, The Science of the total environment,
789 636, 1344–1354, doi:10.1016/j.scitotenv.2018.04.261, 2018.
790 Guedron, S., Grangeon, S., Lanson, B., and Grimaldi, M.: Mercury speciation in a tropical soil association; Conse-
791 quence of gold mining on Hg distribution in French Guiana, Geoderma, 153, 331–346,
792 doi:10.1016/j.geoderma.2009.08.017, 2009.
793 Gygax, S., Gfeller, L., Wilcke, W., and Mestrot, A.: Emerging investigator series: mercury mobility and methylmer-
794 cury formation in a contaminated agricultural flood plain: influence of flooding and manure addition, Environ-
795 mental science. Processes & impacts, 21, 2008–2019, doi:10.1039/c9em00257j, 2019.
796 Haitzer, M., Aiken, G. R., and Ryan, J. N.: Binding of mercury(II) to dissolved organic matter: the role of the mer-
797 cury-to-DOM concentration ratio, Environmental science & technology, 36, 3564–3570,
798 doi:10.1021/es025699i, 2002.
799 Hindersmann, I., Hippler, J., Hirner, A. V., and Mansfeldt, T.: Mercury volatilization from a floodplain soil during a
800 simulated flooding event, J Soils Sediments, 14, 1549–1558, doi:10.1007/s11368-014-0908-2, 2014.
801 Hofacker, A. F., Behrens, S., Voegelin, A., Kaegi, R., Lösekann-Behrens, T., Kappler, A., and Kretzschmar, R.:
802 Clostridium Species as Metallic Copper-Forming Bacteria in Soil under Reducing Conditions, Geomicrobiology
803 Journal, 32, 130–139, doi:10.1080/01490451.2014.933287, 2015.
804 Hofacker, A. F., Voegelin, A., Kaegi, R., and Kretzschmar, R.: Mercury mobilization in a flooded soil by incorpora-
805 tion into metallic copper and metal sulfide nanoparticles, Environmental science & technology, 47, 7739–7746,
806 doi:10.1021/es4010976, 2013.
807 Hojdová, M., Rohovec, J., Chrastný, V., Penížek, V., and Navrátil, T.: The influence of sample drying procedures on
808 mercury concentrations analyzed in soils, Bulletin of environmental contamination and toxicology, 94, 570–
809 576, doi:10.1007/s00128-015-1521-9, 2015.
810 Horvat, M., Nolde, N., Fajon, V., Jereb, V., Logar, M., Lojen, S., Jacimovic, R., Falnoga, I., Liya, Q., Faganeli, J.,
811 and Drobne, D.: Total mercury, methylmercury and selenium in mercury polluted areas in the province Gui-
812 zhou, China, Science of The Total Environment, 304, 231–256, doi:10.1016/S0048-9697(02)00572-7, 2003.
813 Hu, H., Li, M., Wang, G., Drosos, M., Li, Z., Hu, Z., and Xi, B.: Water-soluble mercury induced by organic
814 amendments affected microbial community assemblage in mercury-polluted paddy soil, Chemosphere, 236,
815 124405, doi:10.1016/j.chemosphere.2019.124405, 2019.

816 Jiang, T., Skyllberg, U., Wei, S., Wang, D., Lu, S., Jiang, Z., and Flanagan, D. C.: Modeling of the structure-specific
817 kinetics of abiotic, dark reduction of Hg(II) complexed by O/N and S functional groups in humic acids while
818 accounting for time-dependent structural rearrangement, Geochimica et Cosmochimica Acta, 154, 151–167,
819 doi:10.1016/j.gca.2015.01.011, 2015.
820 Jiskra, M., Wiederhold, J. G., Skyllberg, U., Kronberg, R.-M., and Kretzschmar, R.: Source tracing of natural organ-
821 ic matter bound mercury in boreal forest runoff with mercury stable isotopes, Environmental science. Processes
822 & impacts, 19, 1235–1248, doi:10.1039/c7em00245a, 2017.
823 Jones, M. E., Nico, P. S., Ying, S., Regier, T., Thieme, J., and Keiluweit, M.: Manganese-Driven Carbon Oxidation
824 at Oxic-Anoxic Interfaces, Environmental science & technology, 52, 12349–12357,
825 doi:10.1021/acs.est.8b03791, 2018.
826 Jonsson, S., Skyllberg, U., Nilsson, M. B., Westlund, P.-O., Shchukarev, A., Lundberg, E., and Björn, E.: Mercury
827 methylation rates for geochemically relevant Hg(II) species in sediments, Environmental science & technology,
828 46, 11653–11659, doi:10.1021/es3015327, 2012.
829 Kronberg, R.-M., Jiskra, M., Wiederhold, J. G., Björn, E., and Skyllberg, U.: Methyl Mercury Formation in
830 Hillslope Soils of Boreal Forests: The Role of Forest Harvest and Anaerobic Microbes, Environmental science
831 & technology, 50, 9177–9186, doi:10.1021/acs.est.6b00762, 2016.
832 Lazareva, O., Sparks, D. L., Landis, R., Ptacek, C. J., and Ma, J.: Investigation of legacy industrial mercury in
833 floodplain soils: South River, Virginia, USA, Environ Earth Sci, 78, doi:10.1007/s12665-019-8253-9, 2019.
834 Li, H., Zheng, D., Zhang, X., Niu, Z., Ma, H., Zhang, S., and Wu, C.: Total and Methylmercury of Suaeda heterop-
835 tera Wetland Soil Response to a Salinity Gradient Under Wetting and Drying Conditions, Bulletin of environ-
836 mental contamination and toxicology, 104, 778–785, doi:10.1007/s00128-020-02874-1, 2020.
837 Li, M., Drosos, M., Hu, H., He, X., Wang, G., Zhang, H., Hu, Z., and Xi, B.: Organic amendments affect dissolved
838 organic matter composition and mercury dissolution in pore waters of mercury-polluted paddy soil, Chemo-
839 sphere, 232, 356–365, doi:10.1016/j.chemosphere.2019.05.234, 2019.
840 Liang, X., Lu, X., Zhao, J., Liang, L., Zeng, E. Y., and Gu, B.: Stepwise Reduction Approach Reveals Mercury
841 Competitive Binding and Exchange Reactions within Natural Organic Matter and Mixed Organic Ligands, En-
842 vironmental science & technology, 53, 10685–10694, doi:10.1021/acs.est.9b02586, 2019.
843 Liu, S., Wang, J., Pu, S., Blagodatskaya, E., Kuzyakov, Y., and Razavi, B. S.: Impact of manure on soil biochemical
844 properties: A global synthesis, The Science of the total environment, 745, 141003,
845 doi:10.1016/j.scitotenv.2020.141003, 2020.
846 Liu, Y.-R., Dong, J.-X., Han, L.-L., Zheng, Y.-M., and He, J.-Z.: Influence of rice straw amendment on mercury
847 methylation and nitrification in paddy soils, Environmental pollution (Barking, Essex 1987), 209, 53–59,
848 doi:10.1016/j.envpol.2015.11.023, 2016.
849 Ma, D., Wu, J., Yang, P., and Zhu, M.: Coupled Manganese Redox Cycling and Organic Carbon Degradation on
850 Mineral Surfaces, Environmental science & technology, doi:10.1021/acs.est.0c02065, 2020.
851 Manceau, A., Lemouchi, C., Enescu, M., Gaillot, A.-C., Lanson, M., Magnin, V., Glatzel, P., Poulin, B. A., Ryan, J.
852 N., Aiken, G. R., Gautier-Luneau, I., and Nagy, K. L.: Formation of Mercury Sulfide from Hg(II)-Thiolate

Complexes in Natural Organic Matter, Environmental science & technology, 49, 9787–9796, doi:10.1021/acs.est.5b02522, 2015.

Manceau, A., Nagy, K. L., Marcus, M. A., Lanson, M., Geoffroy, N., Jacquet, T., and Kirpichtchikova, T.: Formation of metallic copper nanoparticles at the soil-root interface, Environmental science & technology, 42, 1766–1772, doi:10.1021/es072017o, 2008.

Marvin-DiPasquale, M., Windham-Myers, L., Agee, J. L., Kakouros, E., Le Kieu, H., Fleck, J. A., Alpers, C. N., and Stricker, C. A.: Methylmercury production in sediment from agricultural and non-agricultural wetlands in the Yolo Bypass, California, USA, The Science of the total environment, 484, 288–299, doi:10.1016/j.scitotenv.2013.09.098, 2014.

Miller, C. L., Mason, R. P., Gilmour, C. C., and Heyes, A.: Influence of dissolved organic matter on the complexation of Hg under sulfidic conditions., Environmental Toxicology and Chemistry, 26, 624–633, 2007.

Miller, C. L., Southworth, G., Brooks, S., Liang, L., and Gu, B.: Kinetic controls on the complexation between mercury and dissolved organic matter in a contaminated environment, Environmental science & technology, 43, 8548–8553, doi:10.1021/es901891t, 2009.

Neculita, C.-M., Zagury, G. J., and Deschênes, L.: Mercury speciation in highly contaminated soils from chlor-alkali plants using chemical extractions, Journal of environmental quality, 34, 255–262, 2005.

Pham, A. L.-T., Morris, A., Zhang, T., Ticknor, J., Levard, C., and Hsu-Kim, H.: Precipitation of nanoscale mercuric sulfides in the presence of natural organic matter: Structural properties, aggregation, and biotransformation, Geochimica et Cosmochimica Acta, 133, 204–215, doi:10.1016/j.gca.2014.02.027, 2014.

Ponting, J., Kelly, T. J., Verhoef, A., Watts, M. J., and Sizmur, T.: The impact of increased flooding occurrence on the mobility of potentially toxic elements in floodplain soil - A review, The Science of the total environment, 754, 142040, doi:10.1016/j.scitotenv.2020.142040, 2020.

Poulin, B. A., Aiken, G. R., Nagy, K. L., Manceau, A., Krabbenhoft, D. P., and Ryan, J. N.: Mercury transformation and release differs with depth and time in a contaminated riparian soil during simulated flooding, Geochimica et Cosmochimica Acta, 176, 118–138, doi:10.1016/j.gca.2015.12.024, 2016.

Poulin, B. A., Gerbig, C. A., Kim, C. S., Stegemeier, J. P., Ryan, J. N., and Aiken, G. R.: Effects of Sulfide Concentration and Dissolved Organic Matter Characteristics on the Structure of Nanocolloidal Metacinnabar, Environmental science & technology, 51, 13133–13142, doi:10.1021/acs.est.7b02687, 2017.

Qiu, G., Feng, X., Wang, S., and Shang, L.: Mercury and methylmercury in riparian soil, sediments, mine-waste calcines, and moss from abandoned Hg mines in east Guizhou province, southwestern China, Applied Geochemistry, 20, 627–638, doi:10.1016/j.apgeochem.2004.09.006, 2005.

Ravichandran, M.: Interactions between mercury and dissolved organic matter--a review, Chemosphere, 55, 319–331, doi:10.1016/j.chemosphere.2003.11.011, 2004.

Ravichandran, M., Aiken, G. R., Reddy, M. M., and Ryan, J. N.: Enhanced Dissolution of Cinnabar (Mercuric Sulfide) by Dissolved Organic Matter Isolated from the Florida Everglades, Environ. Sci. Technol., 32, 3305–3311, doi:10.1021/es9804058, 1998.

Ravichandran, M., Aiken, G. R., Ryan, J. N., and Reddy, M. M.: Inhibition of Precipitation and Aggregation of Metacinnabar (Mercuric Sulfide) by Dissolved Organic Matter Isolated from the Florida Everglades, Environ. Sci. Technol., 33, 1418–1423, doi:10.1021/es9811187, 1999.

Remucal, C. K. and Ginder-Vogel, M.: A critical review of the reactivity of manganese oxides with organic contaminants, Environmental science. Processes & impacts, 16, 1247–1266, doi:10.1039/c3em00703k, 2014.

Richner, W. and Sinaj, S.: Grundlagen für die Düngung landwirtschafltlicher Kulturen in der Schweiz (GRUD 2017), Agroscope, Bern, Schweiz, 276 pp., 2017.

Rivera, N. A., Bippus, P. M., and Hsu-Kim, H.: Relative Reactivity and Bioavailability of Mercury Sorbed to or Coprecipitated with Aged Iron Sulfides, Environmental science & technology, 53, 7391–7399, doi:10.1021/acs.est.9b00768, 2019.

Siemens, J. and Kaupenjohann, M.: Dissolved organic carbon is released from sealings and glues of pore-water samplers, Soil Science Society of America Journal, 67, 795–797, 2003.

Singer, M. B., Harrison, L. R., Donovan, P. M., Blum, J. D., and Marvin-DiPasquale, M.: Hydrologic indicators of hot spots and hot moments of mercury methylation potential along river corridors, The Science of the total environment, 568, 697–711, doi:10.1016/j.scitotenv.2016.03.005, 2016.

Skyllberg, U.: Competition among thiols and inorganic sulfides and polysulfides for Hg and MeHg in wetland soils and sediments under suboxic conditions: Illumination of controversies and implications for MeHg net production, J. Geophys. Res., 113, n/a-n/a, doi:10.1029/2008JG000745, 2008.

Skyllberg, U., Bloom, P. R., Qian, J., Lin, C.-M., and Bleam, W. F.: Complexation of mercury(II) in soil organic matter: EXAFS evidence for linear two-coordination with reduced sulfur groups, Environmental science & technology, 40, 4174–4180, doi:10.1021/es0600577, 2006.

Skyllberg, U. and Drott, A.: Competition between disordered iron sulfide and natural organic matter associated thiols for mercury(II)-an EXAFS study, Environmental science & technology, 44, 1254–1259, doi:10.1021/es902091w, 2010.

Sunda, W. G. and Kieber, D. J.: Oxidation of humic substances by manganese oxides yields low-molecular-weight organic substrates, Nature, 367, 62-64, 1994.

Tang, W., Hintelmann, H., Gu, B., Feng, X., Liu, Y., Gao, Y., Zhao, J., Zhu, H., Lei, P., and Zhong, H.: Increased Methylmercury Accumulation in Rice after Straw Amendment, Environmental science & technology, 53, 6144–6153, doi:10.1021/acs.est.8b07145, 2019.

Tang, Z., Fan, F., Wang, X., Shi, X., Deng, S., and Wang, D.: Mercury in rice (Oryza sativa L.) and rice-paddy soils under long-term fertilizer and organic amendment, Ecotoxicology and environmental safety, 150, 116–122, doi:10.1016/j.ecoenv.2017.12.021, 2018.

Vlassopoulos, D., Kanematsu, M., Henry, E. A., Goin, J., Leven, A., Glaser, D., Brown, S. S., and O'Day, P. A.: Manganese(iv) oxide amendments reduce methylmercury concentrations in sediment porewater, Environmental science. Processes & impacts, 20, 1746–1760, doi:10.1039/c7em00583k, 2018.

Formatted: German (Switzerland)

924 Wang, A. O., Ptacek, C. J., Mack, E. E., and Blowes, D. W.: Impact of multiple drying and rewetting events on
925 biochar amendments for Hg stabilization in floodplain soil from South River, VA, Chemosphere, 262, 127794,
926 doi:10.1016/j.chemosphere.2020.127794, 2021.
927 Wang, A. O., Ptacek, C. J., Paktunc, D., Mack, E. E., and Blowes, D. W.: Application of biochar prepared from
928 ethanol refinery by-products for Hg stabilization in floodplain soil: Impacts of drying and rewetting, Environ-
929 mental pollution (Barking, Essex 1987), 267, 115396, doi:10.1016/j.envpol.2020.115396, 2020.
930 Wang, Y., Chen, Z., Wu, Y., and Zhong, H.: Comparison of methylmercury accumulation in wheat and rice grown
931 in straw-amended paddy soil, The Science of the total environment, 697, 134143,
932 doi:10.1016/j.scitotenv.2019.134143, 2019.
933 Wang, Y., Dang, F., Zhong, H., Wei, Z., and Li, P.: Effects of sulfate and selenite on mercury methylation in a mer-
934 cury-contaminated rice paddy soil under anoxic conditions, Environmental science and pollution research inter-
935 national, 23, 4602–4608, doi:10.1007/s11356-015-5696-8, 2016.
936 Weber, F.-A., Voegelin, A., Kaegi, R., and Kretzschmar, R.: Contaminant mobilization by metallic copper and metal
937 sulphide colloids in flooded soil, Nature Geoscience, 2, 267–271, doi:10.1038/ngeo476, 2009.
938 Zhang, T., Kim, B., Levard, C., Reinsch, B. C., Lowry, G. V., Deshusses, M. A., and Hsu-Kim, H.: Methylation of
939 mercury by bacteria exposed to dissolved, nanoparticulate, and microparticulate mercuric sulfides, Environmen-
940 tal science & technology, 46, 6950–6958, doi:10.1021/es203181m, 2012.
941 Zhang, Y., Liu, Y.-R., Lei, P., Wang, Y.-J., and Zhong, H.: Biochar and nitrate reduce risk of methylmercury in soils
942 under straw amendment, The Science of the total environment, 619-620, 384–390,
943 doi:10.1016/j.scitotenv.2017.11.106, 2018.
944 Zhao, J.-Y., Ye, Z.-H., and Zhong, H.: Rice root exudates affect microbial methylmercury production in paddy soils,
945 Environmental pollution (Barking, Essex 1987), 242, 1921–1929, doi:10.1016/j.envpol.2018.07.072, 2018.
946 Zhu, H., Zhong, H., and Wu, J.: Incorporating rice residues into paddy soils affects methylmercury accumulation in
947 rice, Chemosphere, 152, 259–264, doi:10.1016/j.chemosphere.2016.02.095, 2016.
948

Table 1: List of soil parameters for the two incubated soils (HMLC and LMHC) and manure (MNR). Uncertainties are given as 1σ standard deviation of triplicate experiments (method triplicates).

Parameter	Unit (dry.wt.)	**Cornfield (HMLC)**		**Pasture field (LMHC)**		**Cow Manure (MNR)**	
Land use		Corn field		Pasture		-	
Depth		0 - 20 cm		0 - 20 cm		-	
Soil Type (WRB)		Fluvisol Gleyic		Fluvisol Gleyic		-	
pH_{CaCl2}		8.16		7.84		-	
Water content	(wt. %)	13.8		8.5		90.3	
		Concentration	SD	Concentration	SD	Concentration	SD
C_{org}	wt. %	1.92	0.01	3.45	0.01	45.22	0.09
N_{tot}	wt. %	0.181	0.001	0.372	0.002	3.68	0.08
C_{org}/N_{tot}	-	10.61	-	9.29	-	-	-
S	g kg^{-1}	0.63	0.05	0.77	0.05	3.7	0.1
Hg	mg kg^{-1}	47.3	0.5	2.4	0.3	0.045	0.001
MeHg	µg/kg	26.9	0.2	6.4	0.2	<0.02	-
MeHg/Hg	%	0.06	-	0.28	-	-	-
Al	wt. %	0.91	0.05	1.05	0.04	0.0106	0.0003
Fe		1.95	0.07	2.38	0.05	0.0336	0.0009
Mg		1.25	0.07	1.39	0.05	0.49	0.03
Mn	mg kg^{-1}	493	21	672	38	53	1
P		1169	80	1044	85	8245	232
Cr		56	4	64	5	0.68	0.01
Co		10.75	0.06	11.22	0.43	0.4	0.2
Ni		81.7	0.8	78.3	2.9	2.3	0.1
Cu		40.1	1.2	28.0	0.7	13.1	0.6
Zn		61.8	0.5	47.3	2.0	81	3
As		11.74	0.07	16.04	0.72	0.8	0.4
Cd		0.21	0.04	0.17	0.01	0.042	0.004
Pb		20.8	0.5	18.34	0.5	-	-
V		17.2	0.4	20.99	1.1	0.31	0.01
Sr		137	2	202	6	45.9	1.6
Cs		1.99	0.02	1.52	0.04	-	-
Ba		60.2	1.1	76.9	1.6	9.1	0.5
Ce		7.0	0.4	8.6	0.6	-	-
Gd		0.94	0.03	1.00	0.05	0.021	0.001
U		1.74	0.08	1.29	0.01	0.19	0.01
Hg/Cu molar	‰	366.3	-	25.73	-	-	-
Hg/Mn molar		25.758	-	0.926	-	-	-
Hg/C_{org} molar		0.147	-	0.004	-	-	-
Mn/C_{org} molar		0.0056	-	0.0042	-	-	-

Table 2: Description of the symbols and terms used for different filter fractions in the publication. The particulate fraction is calculated as the difference of the 20 nm and the 10µm filtrate concentrations.

Filter Type	Filter size	Symbol (e.g. $HgT_{\diamond}$)	Description
Suction Cup	10 µm	$HgT_{<10\mu m}$	Soil solution sampled directly from the suction cup contains a variety of particles (clay minerals, bacteria, Mn-/Fe-hydroxides, POM aggregates etc.). We refer to this fraction by adding the ~~suffix~~ subscripts <10µm to the analyte symbol.
Syringe Filter	0.02 µm	$HgT_{<0.02\mu m}$	Soil solution <0.02µm is a cutoff size that may still carry colloids. We refer to this fraction by adding the ~~suffix~~ subscripts <0.02µm to the analyte symbol.
"	-	$P\text{-}HgT_{\Delta}$	Particulate Hg is calculated as: $PHg = Hg_{<10\mu m} - Hg_{<0.02\mu m}$
"	-	$P\text{-}HgT_{rel.}$	Relative particulate Hg is calculated as: $PHg_{rel.} = (Hg_{<10\mu m} - Hg_{<0.02\mu m})/Hg_{<10\mu m}$
AF4 membrane	1 kDa	$HgT_{<1kDa}$	Molecules in solution under this cutoff size are not expected to have colloidal properties. Therefore, this range is referred to as "truly dissolved" in the text.

Formatted: Font: (Default) Times New Roman
Formatted Table
Formatted: Font: (Default) Times New Roman
Formatted: Font: (Default) Times New Roman
Formatted: Font: (Default) Times New Roman
Formatted: Font: (Default) Times New Roman
Formatted: Font: (Default) Times New Roman,
Formatted: Font: (Default) Times New Roman
Formatted: Font: (Default) Times New Roman
Formatted: Font: (Default) Times New Roman

Table 3: Soil MeHg concentrations and net-methylation (MeHg/Hg) over the time of the experiment.

Treatment	day	n	Mean MeHg (µg kg^{-1})	SD MeHg (µg kg^{-1})	Range MeHg (µg kg^{-1})	MeHg/Hg (‰)	net MeHg productionde /methylation (%)
HMLC	0	1	26.9	-	26.9 - 26.9	0.57	-
	14	3	30.14	2.19	28.04 - 32.42	0.64	12.0
	28	3	52.04	10.65	39.74 - 58.25	1.1	73.1
	42	3	30.03	5.05	26.93 - 35.86	0.75	32.4
HMLC +MNR	0	1	26.9	-	26.9 - 26.9	0.57	-
	14	3	43.41	1.99	42 - 44.81	1.03	81.1
	28	3	57.79	13.79	41.88 - 66.41	1.24	20.7
	42	3	30.94	3.43	28.85 - 34.9	0.67	45.9
LMHC	0	1	6.4	-	6.4 - 6.4	2.72	-
	14	3	8.11	1.09	7.33 - 9.36	2.99	10.0
	28	3	12.07	1.1	10.81 - 12.87	4.11	37.2
	42	3	7.95	0.35	7.73 - 8.36	3.42	16.7
LMHC +MNR	0	1	6.4	-	6.4 - 6.4	2.69	-
	14	3	10.86	1.86	8.76 - 12.32	3.72	38.1
	28	3	14.31	0.17	14.12 - 14.43	4.7	26.6
	42	3	8.4	0.09	8.33 - 8.5	3.67	22.0

Formatted: Left

Formatted: Font: (Default) Times New Roman

Formatted Table

Formatted: Font: (Default) Times New Roman

Formatted: Font: (Default) Times New Roman

Formatted: Font: (Default) Times New Roman

Formatted: Font: (Default) Times New Roman

Formatted: Font: (Default) Times New Roman

Formatted: Font: (Default) Times New Roman

Formatted: Font: (Default) Times New Roman

Formatted: Font: (Default) Times New Roman

Formatted: Font: (Default) Times New Roman

Formatted: Font: (Default) Times New Roman

Formatted: Font: (Default) Times New Roman

Formatted: Font: (Default) Times New Roman

Formatted: Font: (Default) Times New Roman

Formatted: Font: (Default) Times New Roman

Formatted: Font: (Default) Times New Roman

Formatted: Font: (Default) Times New Roman

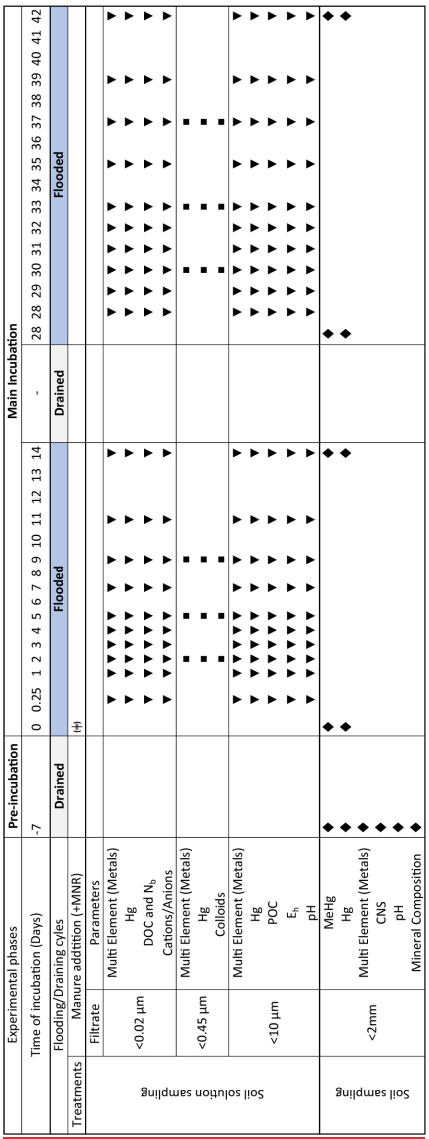

Figure 1 Schedule of preformed incubation experiment, samplings and measurements: Blue bars indicate soil flooding periods. Gray bars represent drained periods. The width of the columns is not proportional to the time of incubation. In the treatments row the (±) symbol indicates the addition of liquid manure to the microcosms specifically treated with manure (+MNR). Triangles represent regular soil solution sampling points. Rectangles represent soil solution sampling for colloid analyses. Diamonds represent time points for soil sampling. At -7 days, soil was sampled from the pooled soil directly before the pre-incubation.

Formatted: Caption, Right: 0.01 cm, Space After: 0 pt, Line spacing: single

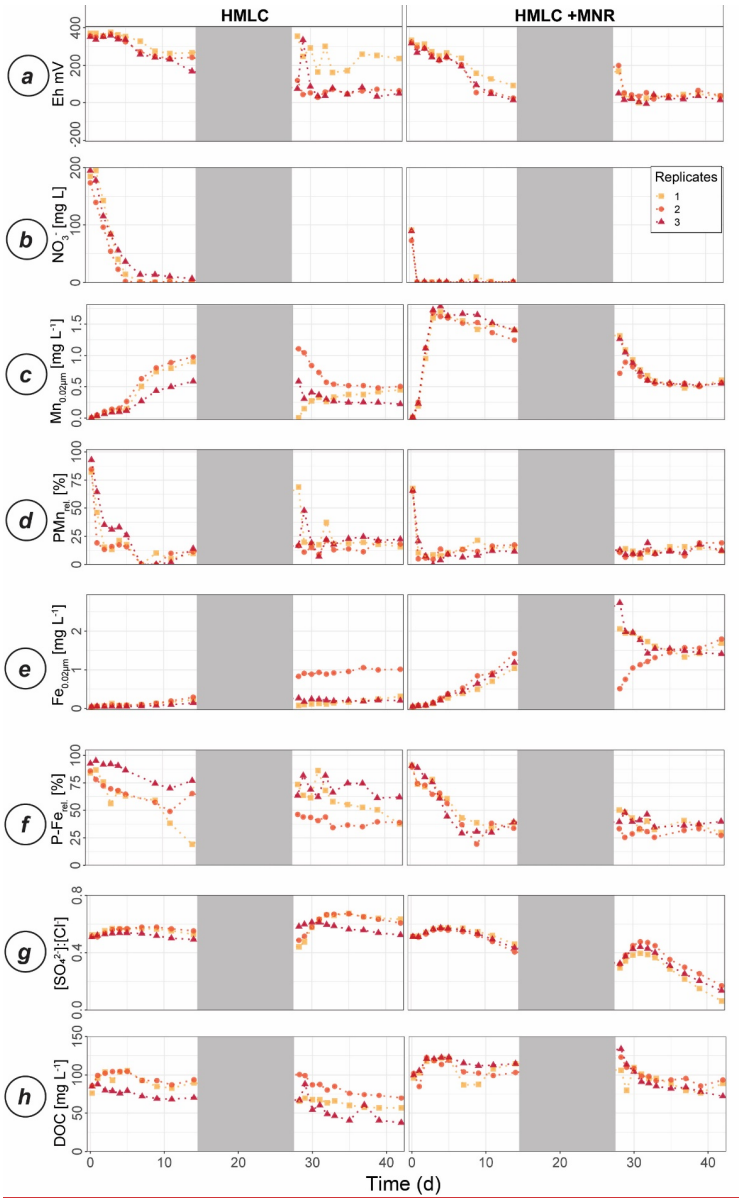

970

971 **Figure 2 Soil solution dynamics in cornfield soil (HMLC) incubations for redox potential (a),**
972 **redox reactive elements (Mn, PMn, Fe, P-Fe, $[SO_4^{2-}]$:[Cl⁻]) (b-f) and dissolved organic carbon**
973 **(h). Lines between points were plotted to improve readability. The gray area indicates the**
974 **drained period.**

Formatted: Caption, Right: 3.51 cm, Space After: 0 pt, Line spacing: single

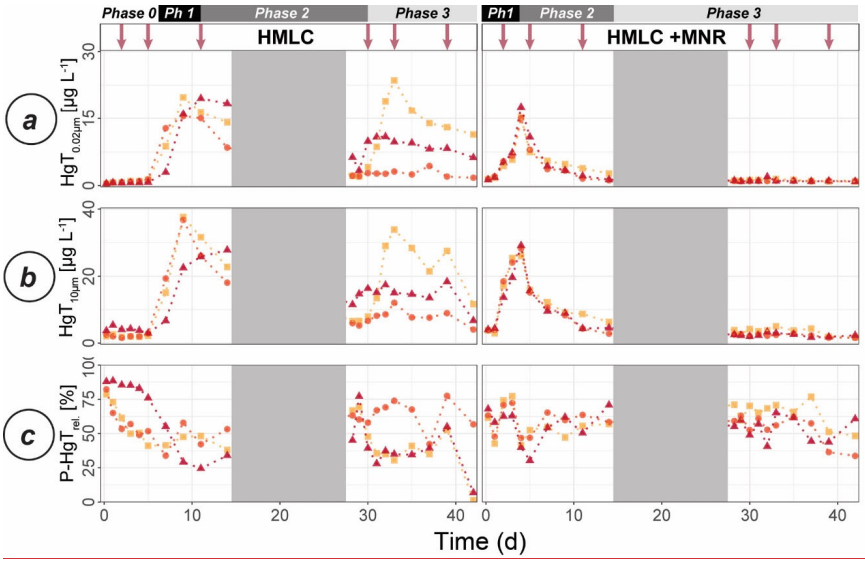

975

976 Figure 3 Soil solution dynamics in cornfield soil (HMLC) incubations for Hg (a-c) subdivided in phases (0-3).
977 Lines between points were plotted to improve readability. The gray area indicates the drained period. Red ar-
978 rows indicate sampling days for AF4-ICP-MS analyses.

979

980

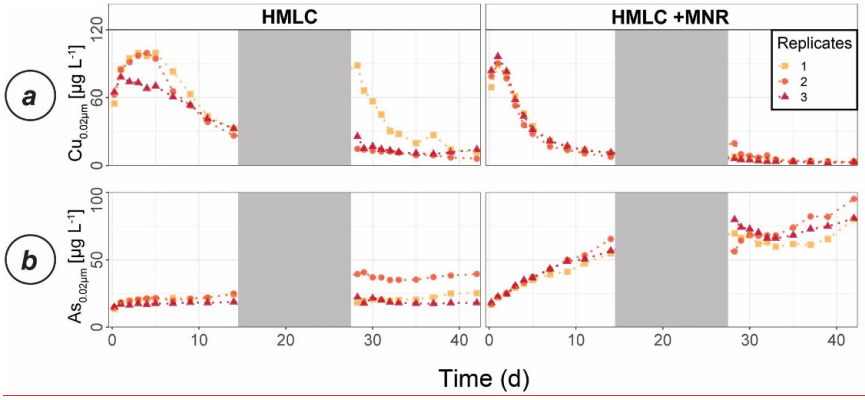

981

982 Figure 4 Soil solution dynamics in cornfield soil (HMLC) incubations for Cu (a) and As (b). Lines between
983 points were plotted to improve readability. The gray area indicates the drained period.

984

985

Formatted: Right: 1.26 cm

Formatted: Right: 1.51 cm

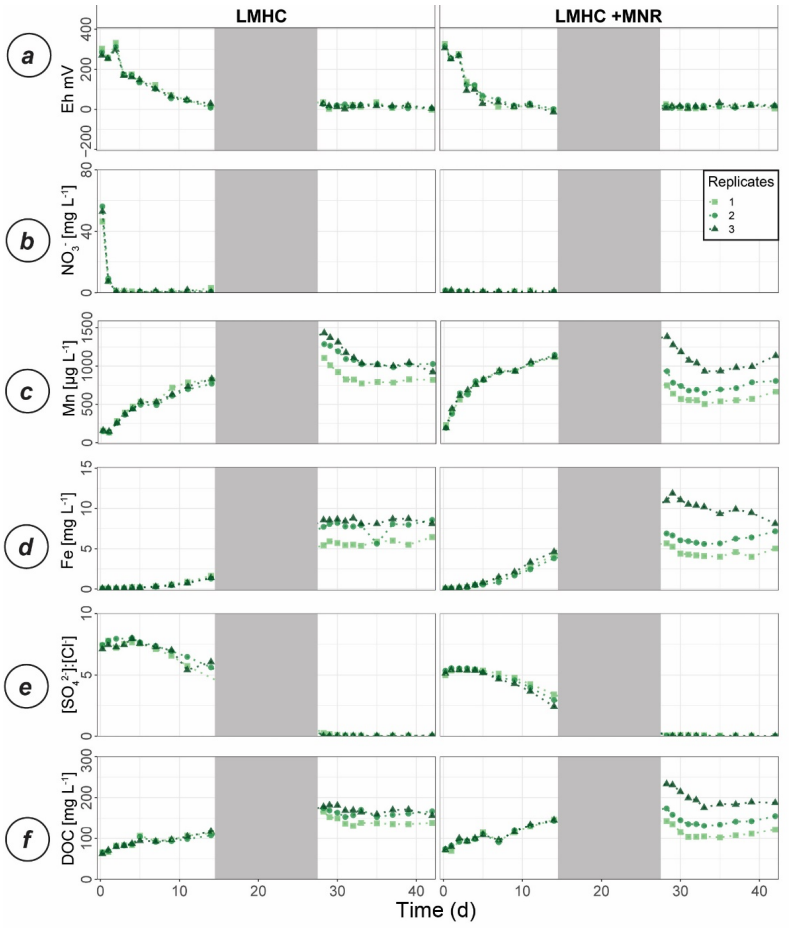

986

987 **Figure 5 Soil solution dynamics in pasture field soil (LMHC) incubations for redox potential (a), redox**
988 **reactive elements (Mn, PMn, Fe, P-Fe, [SO_4^{2-}]:[Cl^-]) (b-f) and dissolved organic carbon (h). Lines be-**
989 **tween points were plotted to improve readability. The gray area indicates the drained period.**

990

Formatted: Right: 2.51 cm, Tab stops: 11 cm, Left + 12.75 cm, Left

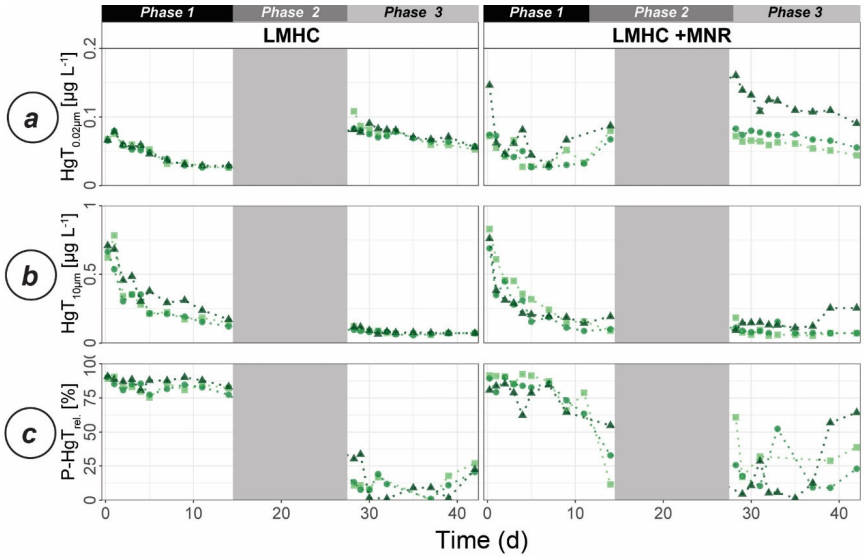

Figure 6 Soil solution dynamics in pasture field soil (LMHC) incubations for Hg (a-c) subdivided in phases (1-3). Lines between points were plotted to improve readability. The gray area indicates the drained period.

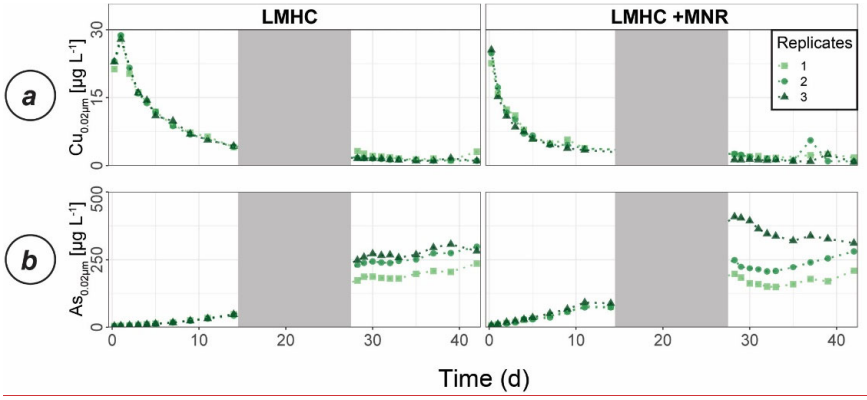

Figure 7 Soil solution dynamics in pasture field soil (LMHC) incubations for Cu (a) and As (b). Lines between points were plotted to improve readability. The gray area indicates the drained period.

Formatted: Right: 1.51 cm

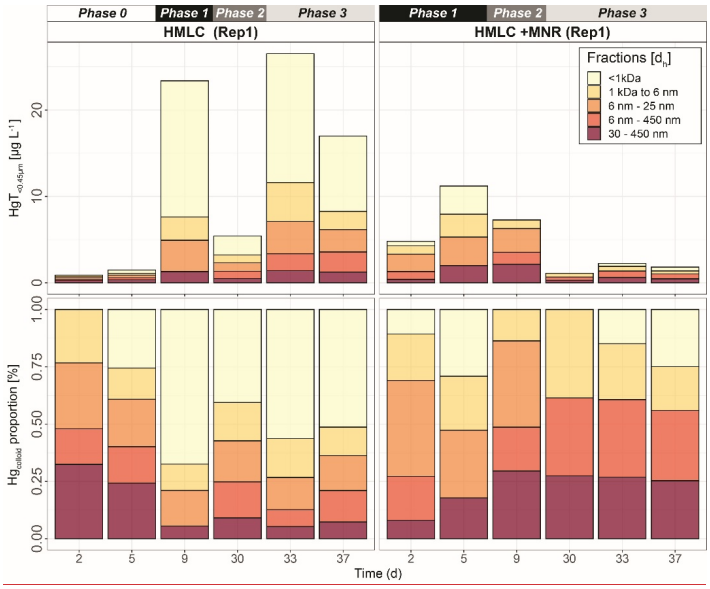

Figure 8 Size distribution of Hg estimated after AF4 fractogram deconvolution for Rep1 of cornfield soil incubation (HMLC and HMLC +MNR) subdivided in phases (0-3). The concentration of HgT in size fractions was calculated using an external calibration of the ICP–MS directly after the AF4 run. The concentration of HgT in "< 1kDa" was calculated by subtracting the sum of the fractions from the HgT concentration in the same sample measured separately by ICP–MS. The fractograms of all analysed time points are shown in the supplement (Figs. S9-S12).

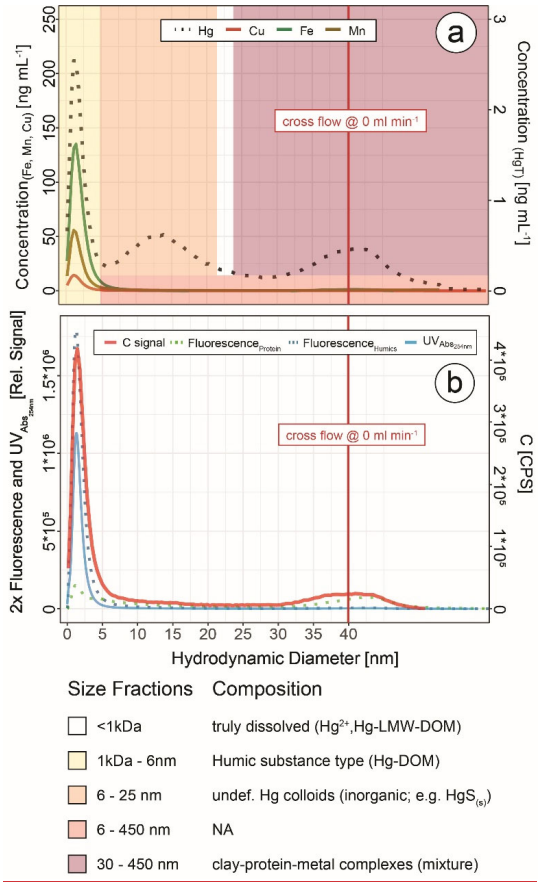

Figure 9 Hg, Cu, Mn and Fe concentrations (a) and C signals (ICP–MS), UV_{254nm} absorbance and fluorescence signals (b) in colloids as a function of hydrodynamic diameter (related to retention times on AF4) in a sample from HMLC at day 9 after flooding. These fractograms were obtained at linearly decreasing crossflow from 2 to 0 mL min^{-1} over 20 min. The red line indicates the time point where the crossflow reached 0 ml min^{-1}. Areas (yellow to red color) indicate size fraction ranges assigned during deconvolution.

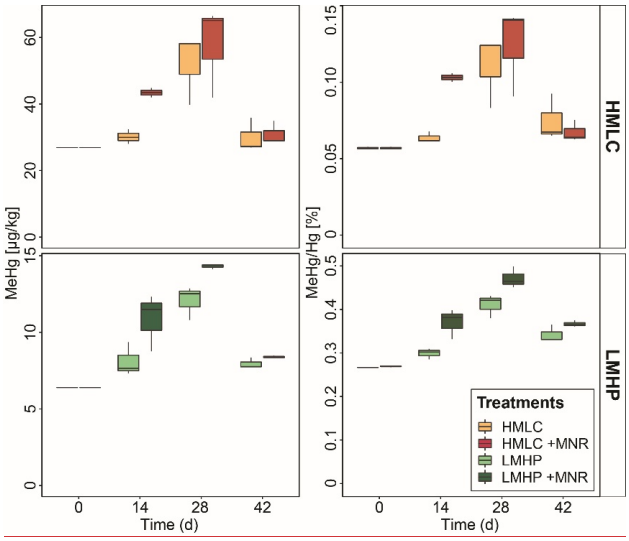

Figure 10 Soil MeHg concentrations and MeHg/Hg ratios over the course of the experiment for corn field soils (HMLC, yellow/red) and pasture field soils (LMHC, lime/green). Highest net methylation was observed during first flooding for +MNR treatments and during the draining period for microcosms without manure addition. A significant decrease of MeHg/Hg was observed during the second flooding for all treatments.

Formatted: Right: 5.51 cm, Tab stops: 8.75 cm, Left + Not at 10.5 cm

Formatted

Formatted: Justified